

Mass Spectrometric Fingerprints of Organic Compounds in Sulfate-Rich Ice Grains: Implications for Europa Clipper

Maryse Napoleoni^{1}, Fabian Klenner^{1,2}, Lucía Hortal Sánchez¹, Nozair Khawaja¹, Jon K. Hillier¹, Murthy S. Gudipati³, Kevin P. Hand³, Sascha Kempf⁴, Frank Postberg¹*

¹Institute of Geological Sciences, Freie Universität Berlin, Berlin 12249, Germany

²Department of Earth and Space Sciences, University of Washington, Seattle, WA 98195, USA

³Science Division, Jet Propulsion Laboratory, California Institute of Technology, Pasadena, CA 91109, USA

⁴LASP, University of Colorado, Boulder, CO 80303, USA

KEYWORDS

Ocean worlds, Space missions, SUDA, Analogue experiments, LILBID, salt effects, Icy moons

ABSTRACT

The surface ice of Europa is known to contain high proportions of inorganic material that could heavily influence the compositional analysis of organic compounds in ejecta ice grains by the Surface Dust Analyzer (SUDA) impact ionization mass spectrometer onboard NASA's Europa Clipper mission. We previously have analyzed the effects of NaCl^{1,2} on the mass spectral appearance of organic-rich ice grains. Here we present analogue experiments for SUDA simulating cation and anion mass spectra of organic-rich ice grains together with sulfates, one of the most abundant inorganic compounds on Europa's surface. Using the Laser Induced Liquid Beam Ion Desorption (LILBID) technique a diverse range of representative organic species in MgSO₄- and H₂SO₄-rich matrices at concentrations ranging from 0.01M to 1M were measured. Results show that mass spectrometric signatures of organic species can be detected in MgSO₄-rich and H₂SO₄-rich ice grains via molecular ions, although the mass spectral appearance changes from molecular ions to a range of adducts with Mg²⁺, OH⁻, HSO₄⁻ ions, and MgSO₄ and H₂SO₄ molecules depending on the matrix and the matrix concentration. Sensitivity to the organics is typically higher in cation mode than anion mode in both matrices. Due to suppression effects, the sensitivity to detect the organics decreases with increasing MgSO₄ concentration; but it does not decrease in H₂SO₄ matrices in cation mode. We establish generic rules for the detection of organics in European ice grains by SUDA, applicable to a wide range of organic species in complex ice matrices. The recorded mass spectra complement a spectral reference database for Europa Clipper and other ocean world missions.

TEXT

1 Introduction

Subsurface oceans have been detected in several icy satellites in the outer solar system, such as Europa^{3,4}, Enceladus⁵, Ganymede⁶ and Callisto⁷. As potentially habitable environments they are at the center of attention of planetary exploration and astrobiology investigations^{8,9}. On Europa, there is intriguing evidence of erupting plumes^{e.g.,10} that might eject water ice grains from subsurface reservoirs to high altitudes. A similar plume has previously been observed at the south pole of Enceladus^{11,12,13,14}. Bombardment by micrometeorites also ejects ice particles from the surface, continuously supplying dust clouds around atmosphereless bodies such as the Galilean moons of Jupiter^{15,16}.

The compositional analysis of such ice grains from Europa will be accomplished by the Surface Dust Analyzer¹⁷ (SUDA) onboard NASA's upcoming Europa Clipper mission¹⁸. SUDA is an impact ionization time-of-flight mass spectrometer (TOF-MS) and the successor instrument of the Cosmic Dust Analyzer¹⁹ (CDA) which detected water²⁰, salts^{21,22,23} and organic material^{24,25,26} in dust grains from Enceladus during the Cassini mission, thus characterizing properties of an extraterrestrial water reservoir. SUDA will be able to detect both cations and anions at a high mass resolution ($m/\Delta m = 200-250$) in the mass range $m = 1-500$ u, and will potentially sample freshly ejected plume material at Europa, enabling the compositional mapping of geological surface features by analysis of surface ejecta^{27,28,29,30}.

SUDA will be able to detect organic material encased in European ice grains. This material may originate from the subsurface ocean and be transported to the surface by tectonic processes (e.g., resurfacing) but it will also be exposed to surface conditions such as radiation processing and S-ion implantation and mixed with salts and other inorganic compounds present in the subsurface ocean and ice crust. Europa's subsurface ocean and surface ice are rich in salts, such as NaCl^{e.g., 31, 32} and sulfates^{e.g., 33,34,35,36}. Magnesium sulfates are likely some of the major salts

in Europa's ice composition and, although exact concentrations are not yet constrained, estimates range from 0.04 to 4.2 mol/kg H₂O^{37,38}. Whereas their distribution has been broadly determined e.g.,^{39,40}, their origin is still debated. On the one hand, the Io plasma torus that interacts with and affects the surface of Europa^{41,42} was found to lack magnesium ions³⁷, suggesting that magnesium ions are likely to originate directly from the subsurface ocean⁴³. Generally, sulfates could be formed abundantly through the differentiation of a subsurface ocean and leaching of chondritic material⁴⁴. On the other hand, they could be a radiation product of exogenic sulfur ions and magnesium salts already present on Europa's surface^{35,39}. Regions experiencing sulfur radiolysis may therefore contain particularly high concentrations of sulfate salts.

Europa's surface ice is exposed to substantial ionizing radiation due to the strong magnetosphere of Jupiter^{45,46}. Several studies have shown that irradiating water ice leads to the production of a variety of radiolytic products, such as H₂ and O₂^{47,48,49,50}. The production of strong oxidants such as H₂O₂ and O₃ is expected on Europa^{e.g.,51,52} but so far only H₂O₂ has been observed on Europa's leading hemisphere^{39,53}. Oxidation reactions are presumed to play a major role in the surface chemistry of Europa's ice⁵⁴. Due to the bombardment of sulfur ions onto the surface, another expected product of radiolytic chemistry is sulfuric acid hydrate H₂SO₄(H₂O)^{53,55,56,57}. Indeed, sulfuric acid hydrates mixed with water ice dominate the surface composition in the trailing hemisphere of Europa, as they are the main product of the surface radiolysis reactions^{56,39,58,59}. Recent ground-based observations at high spectral resolution have confirmed the presence of sulfuric acid on the trailing hemisphere^{39,60}. The concentration of H₂SO₄ in Europa's ice has been estimated to be up to 2.5–3.6 mol/kg H₂O³⁷, but these values are strongly location-dependent^{58,61}.

Laboratory experiments reproducing the impact ionization mass spectra of icy dust grains as produced by SUDA- or CDA-type instruments have been conducted with the Laser Induced

Liquid Beam Ion Desorption^{62,63} (LILBID) technique. This technique has been used to calibrate spaceborne mass spectrometers and reproduce the compositional variations seen in icy moons' water ice particles^{21,25,26,64}. LILBID analog experiments have also been conducted to investigate the mass spectral characteristics of different biosignatures, such as amino acids, fatty acids, peptides and bacterial material, as if enclosed in sampled water ice grains^{1,65,66}. In both LILBID and impact ionization, the analyzed material is exposed to very high energy densities and undergoes a high degree of macroscopic and molecular fragmentation, leading to the formation of charged molecular fragment clusters detectable by time-of-flight mass spectrometry. In both cases, the chemical composition - and not the phase, i.e., liquid or solid - is key in the formation of molecular and elemental ions due to the very high energy density applied to the analyzed material^{21,23,26}. The main difference between the populations of ions created by LILBID vs by impact ionization (for a similar composition of analyzed material) is due to differences in the electric field environment in which the ionization and the formation of molecular clusters and fragments occurs: ions are collected and rapidly accelerated towards the detector in spaceborne impact ionization mass spectrometers, while in LILBID ions drift through a field-free region after they are generated. The selection of ions crossing this field-free region at a certain speed therefore allows the simulation of the speed at which the impact cloud expands in spaceborne impact ionization mass spectrometers and with that the kinetic energy of the impact. This can be achieved by combining variations in laser power density with delay time⁶⁴.

Recently, the LILBID technique was used to investigate the mass spectral fingerprints of a wide range of organic compounds in NaCl-rich water ice grains² as present at Enceladus²¹ and probably Europa³². We showed that despite high salt concentrations, organic material - depending on the NaCl concentration - can be detected via molecular peaks or sodiated and chlorinated adducts². Matrix effects were shown to play an important role on the detectability

of organics and were dependent on the structural and compositional properties of the organic compounds, including the presence of functional groups, and the salt concentration.

Building on these experiments², we here measured LILBID spectra of the same range of organic species (5-amino-1-pentanol, acetic acid, benzoic acid, butylamine, glucose, methanol, pyridine) in both cation and anion mode, to investigate their mass spectral signatures in 0.01, 0.1 and 1M concentration MgSO₄- and H₂SO₄- rich matrices, i.e., concentrations representative of those expected at the surface of Europa and similar as those used for NaCl matrices². The goal of this work is to understand the interactions between salts or sulfuric acid and organics in simulated impact mass spectra of SUDA, for organic content on the order of several % in concentration. We here complement the general rules inferred to predict the mass spectral appearance of organic species in salt-rich ice grains with matrix compound specifically relevant on Europa's surface (MgSO₄ and H₂SO₄) for the analysis of ice grains by SUDA-type impact ionization mass spectrometers.

2 Experimental

2.1 Laser Induced Liquid Beam Ion Desorption (LILBID) Experimental Setup

The LILBID technique (Figure 1), used here to record mass spectra of the different solutions of organic compounds in MgSO₄- and H₂SO₄-rich matrices, is described in detail in Klenner et al.⁶⁴. The sample is injected in a μm-sized liquid water beam into a vacuum chamber (5×10^{-5} mbar) and ionized by irradiation with a pulsed infrared laser ($\lambda = 2840$ nm) at variable laser energies (up to 4 mJ). A time-of-flight (TOF) mass spectrometer then detects and records the created ions with a mass resolution of 600-800 m/Δm. The ion mode (cation or anion) can be chosen by adjusting the polarity of the mass spectrometer's electrodes. Delayed extraction of the ions, as shown in Figure 1, allows the selection of ions of different velocities: after going through a field-free region, ions arriving later than the defined delay time are blocked by the

repeller (applying a potential that prevents them to enter the mass spectrometer detector). Different impact speeds of the ice grains, ranging from 3 to >20km/s, can thus be simulated by adjusting the extraction delay and the laser's power intensity⁶⁴. Before each measurement session, the LILBID setup was calibrated and checked for contamination (e.g., by salts or other organic species that could interfere in the spectra). Ion signals were amplified, digitized and recorded with a LabVIEW-controlled computer. Each recorded spectrum was an average of three hundred individual spectra, co-added to improve the signal-to-noise ratio and baseline-corrected by using an in-house developed Python script based on the Penalized Least Squares Method⁶⁷. The recorded spectra are stored in a database (<https://lilbid-db.planet.fu-berlin.de>) in which analogue data for impact ionization mass spectrometers⁶⁷ is collected and made available.

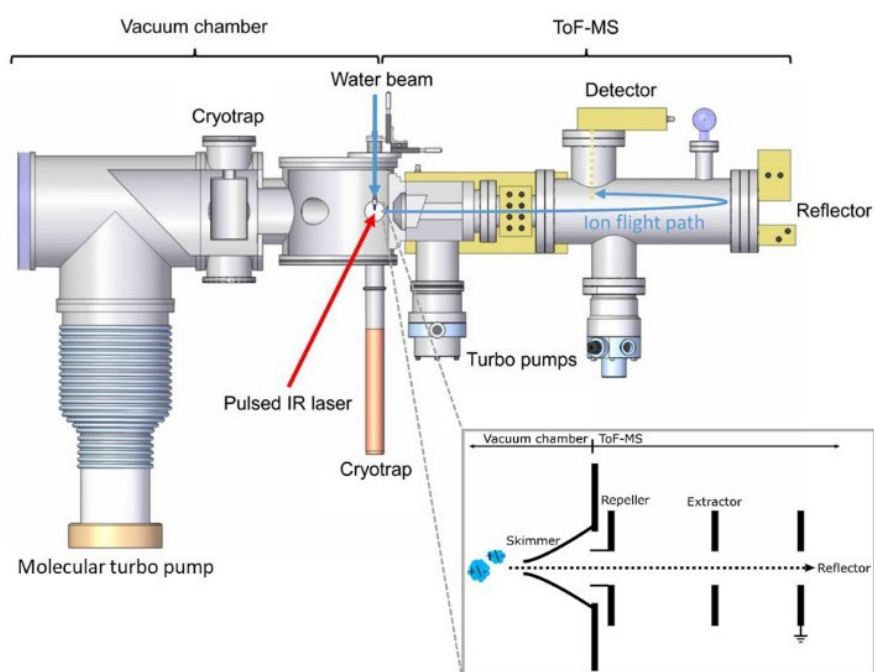
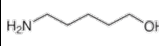
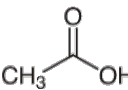
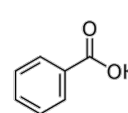

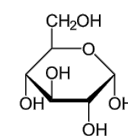
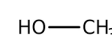
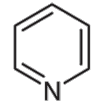


Figure 1. The Laser Induced Liquid Beam Ion Desorption (LILBID) laboratory setup, reproducing the impact ionization mass spectra of ice grains recorded in space (figure reproduced with permission from Klenner et al.⁶⁴. Copyright 2023 John Wiley and Sons). The

principle of delayed extraction of the ions as a function of their initial velocities is shown on the bottom right insert.

2.2 Organic Solutions

Solutions containing both an organic species and MgSO_4 or H_2SO_4 were prepared. The solutions were made in $18.2 \text{ M}\Omega\cdot\text{cm}$ ultrapure water, to which was added either MgSO_4 or H_2SO_4 at different concentrations (0.01M [mol/L], 0.1M and 1M – i.e., concentrations of 1.2 g/L, 12 g/L and 120 g/L for MgSO_4 and of 0.98 g/L, 9.8 g/L, and 98 g/L for H_2SO_4 , respectively). Seven organic species (Table 1), namely 5-amino-1-pentanol ($\text{C}_5\text{H}_{13}\text{NO}$), acetic acid ($\text{C}_2\text{H}_4\text{O}_2$), benzoic acid ($\text{C}_7\text{H}_6\text{O}_2$), butylamine ($\text{C}_4\text{H}_{11}\text{N}$), glucose ($\text{C}_6\text{H}_{12}\text{O}_6$), methanol (CH_4O), and pyridine ($\text{C}_5\text{H}_5\text{N}$), were measured individually. Among those, four species (acetic acid, glucose, methanol, and pyridine) were measured at concentrations of 5 wt% in both matrices; two species (butylamine and 5-amino-1-pentanol) at reduced concentrations of 0.1 wt% and 1.3 wt% respectively when in 1 M H_2SO_4 due to the formation of precipitates; and one species, benzoic acid, measured at 0.17 wt% in all concentrations of both matrices as it is poorly soluble in water. The organic species we investigated cover a wide range of functional groups, namely: hydroxyl, azine, (aromatic) carboxylic acid, (aromatic) amine, and alkanolamine.

		5-amino-1-pentanol	Acetic acid	Benzoic acid	Butylamine	Glucose	Methanol	Pyridine
								
Formula		$\text{C}_5\text{H}_{13}\text{NO}$	$\text{C}_2\text{H}_4\text{O}_2$	$\text{C}_7\text{H}_6\text{O}_2$	$\text{C}_4\text{H}_{11}\text{N}$	$\text{C}_6\text{H}_{12}\text{O}_6$	CH_4O	$\text{C}_5\text{H}_5\text{N}$
Molecular weight (u)		103	60	122	73	180	32	79
Molecular concentrat	All MgSO_4 matrices &	485	833	13.9	685	278	1563	633

ions (mmol/L)	0.01M, 0.1M H ₂ SO ₄							
	1M H ₂ SO ₄ matrix	126	833	13.9	14	278	1563	633
pH in solution	H ₂ O	12.1	2.4	3.3	12.3	7.1	9.0	8.6
	0.01M MgSO ₄	11.9	2.5	3.2	12.1	5.5	7.6	8.7
	0.1M MgSO ₄	10.9	2.5	3.2	11.5	5.6	7.6	8.6
	1M MgSO ₄	9.3	4.16	3.3	9.4	6.2	6.7	8.8
	0.01M H ₂ SO ₄	12.0	2.0	2.1	12.2	1.9	2.0	6.8
	0.1M H ₂ SO ₄	11.0	0.9	1.2	11.2	1.3	1.2	5.8
	1M H ₂ SO ₄	0.4	0.2	0.8	0.4	0.2	0.8	0.8

Table 1. Organic species investigated in the LILBID experiments, their molecular weights, their molecular concentrations and the resulting pH values of the different matrix solutions investigated.

3 Results

We here present the results of the LILBID measurements of the organic species (Table 1) in MgSO₄- and H₂SO₄-rich matrices at 0.01, 0.1 and 1M MgSO₄ or H₂SO₄. Due to the high number of spectra recorded, only part of the data is presented in this manuscript and the supplementary material, with the remainder available in the LILBID database (<https://lilbid-db.planet.fu-berlin.de>). The same organic compounds were previously measured in pure water and NaCl matrices at similar concentrations².

3.1. Spectra of the MgSO₄ Background Matrix

The cation spectra of magnesium sulfate at 0.01M concentration (Figure 2) show a wide range of Mg-bearing cations: [Mg(OH)]⁺, [*n*Mg⁺(OH)_{2*n*-1}]⁺ (i.e., [2Mg⁺(OH)₃]⁺, [3Mg⁺(OH)₅]⁺, [4Mg⁺(OH)₇]⁺, [5Mg⁺(OH)₉]⁺...), [(MgSO₄)₁₋₂+H]⁺, [Mg(OH)(MgSO₄)₁₋₂]⁺ and [*n*Mg⁺(OH)_{2*n*-1}+(MgSO₄)]⁺ species, with *n* > 1. All peaks corresponding to Mg-bearing cations show characteristic Mg isotope patterns (²⁴Mg, ²⁵Mg and ²⁶Mg with intensities of 79%, 10%

and 11% respectively). The cation mass spectra of the 0.1M MgSO₄ solution (Figure S1) show similar peaks of Mg-bearing cations, but at lower intensities and with a smaller number of water clusters. Fewer peaks were detected in 1M MgSO₄ (Figure S2), but [Mg(OH)]⁺ and [nMg+(OH)_{2n-1}]⁺ peaks are still identified.

In anion mode, peaks from deprotonated sulfate ions [(H₂SO₄)_n-H]⁻ and a range of magnesium-containing species were present in the mass spectra of 0.01M and 0.1M MgSO₄ (Figure 3 and Figure S3): [(MgSO₄)_n(OH)]⁻, [(MgSO₄)_nHSO₄]⁻, and [(MgSO₄)_n(H₂SO₄)_m(HSO₄)]⁻. In 1M MgSO₄ the intensities of these peaks were reduced. The sulfite anion [SO₃]⁻, or the [S₂O]⁻ anion, was tentatively detected at m/z 80 in the spectra of 0.1M and 1M MgSO₄ (Figure S3).

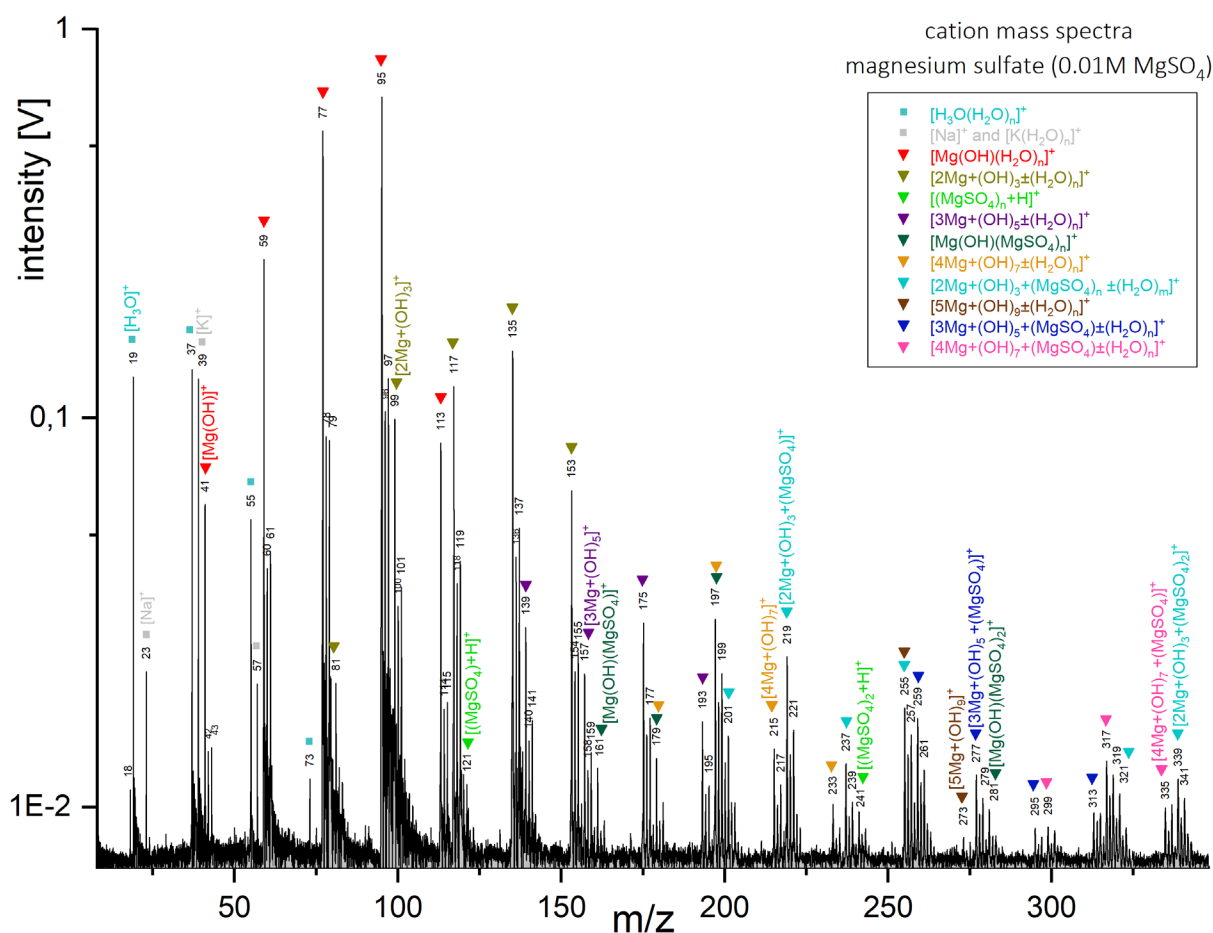


Figure 2. Baseline-corrected cation mass spectrum of magnesium sulfate (MgSO₄) at a concentration of 0.01M, generated with a delay time of 5.0 μs.

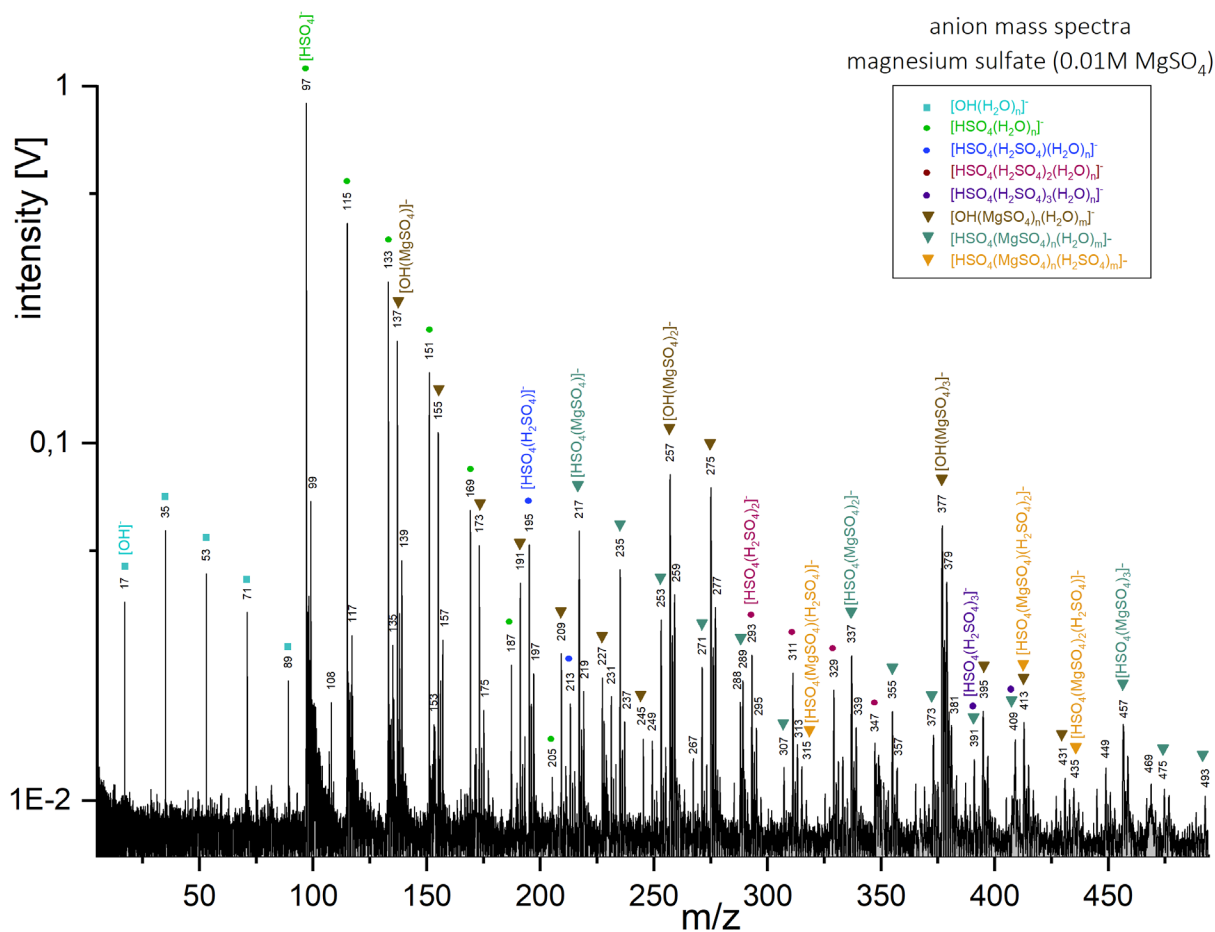


Figure 3. Baseline-corrected anion mass spectrum of magnesium sulfate (MgSO_4) at a concentration of 0.01M, generated with a delay time of 6.3 μs . All peaks related to sulfate only are labeled with circles whereas all species containing magnesium sulfate are labeled with triangles.

3.2 Spectra of Organic Compounds in MgSO_4 -rich Matrix

Cation mode

In cation mode, protonated molecular peaks $[\text{M}+\text{H}]^+$ were detected for all organic species in 0.01M MgSO_4 , for all species except benzoic acid in 0.1M MgSO_4 and only for 5-amino-1-pentanol, methanol and pyridine in 1M MgSO_4 (Table 2). These are the highest intensity peaks in the spectra of 5-amino-1-pentanol (Figure 4, Figures S4 and S5) and pyridine (Figure S6) at all MgSO_4 concentrations, and of butylamine in 0.01M (Figure S7) and 0.1M MgSO_4 .

A wide range of other organic cations containing Mg atoms were detected (Table 2, Figure 4, Figures S4-S12):

- $[M-H+Mg]^+$ cations for all species except 5-amino-1-pentanol, methanol and pyridine;
- $[M+Mg(OH)]^+$ cations for all species except methanol (but tentatively for butylamine);
- $[M+2Mg+(OH)-2H]^+$ ($M+63u$), $[M+3Mg+(OH)_2-H]^+$ ($M+105u$), $[M+4Mg+(OH)_5-H]^+$ ($M+180u$) cations in the spectra of acetic acid in 0.01M and 0.1M $MgSO_4$;
- $[M+2Mg+(OH)_3]^+$ and $[M+3Mg+(OH)_5]^+$ cations in the spectra of benzoic acid in 0.01M $MgSO_4$;
- $[M(SO_3)+3H]^+$, $[M(SO_3)+Mg+H]^+$, $[M(SO_3)(MgSO_4)+Mg+H]^+$ in the spectra of glucose in 0.01M $MgSO_4$;
- $[M+Mg+(OH)_2+H]^+$ and $[2M+Mg+(OH)_2+H]^+$ in the spectra of methanol in 0.01M $MgSO_4$.

The number and intensities of these peaks typically decreased with increasing $MgSO_4$ concentration (Table 2; e.g., Figures S8 and S9).

Addition of $MgSO_4$ molecules onto organic cations was observed in 0.01M $MgSO_4$ for all species except butylamine and methanol, with cations such as $[M(MgSO_4)+H]^+$, $[M(MgSO_4)+Mg-H]^+$ and $[M(MgSO_4)(OH)+Mg]^+$ (Table 2). These species are suppressed at higher $MgSO_4$ concentrations and have only been observed for 5-amino-1-pentanol and tentatively for acetic acid in 0.1M and 1M $MgSO_4$. Addition of H_2SO_4 molecules onto organic cations (i.e., $[nM+(H_2SO_4)+H]^+$ peaks with $n \geq 1$) was observed for 5-amino-1-pentanol in

0.01M and 0.1M MgSO₄ (Figures 4, S4), for pyridine in 0.1M MgSO₄ and tentatively for acetic acid and benzoic acid in 0.01M MgSO₄.

Adducts of molecular organic species and charged fragments thereof ($[M+M-x]^+$ with x a fragment of the organic species) or fragmented polymers of the organics ($[nM-x]^+$ with $n > 1$) were observed in the cation spectra of 5-amino-1-pentanol in 0.01M and 0.1M MgSO₄ (Figures S4, 4), butylamine in 0.01M and 0.1M MgSO₄ (Figure S7), acetic acid in 0.01M MgSO₄ (Figure S8), and glucose in 0.01M MgSO₄ (Figure S12).


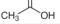
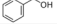

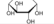
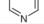
			5-amino-1-pentanol 	Acetic acid 	Benzoic acid 	Butylamine 	Glucose 	Methanol HO—CH ₃	Pyridine 
0.01M MgSO ₄	$[M+H]^+$	<i>M+1 u</i>	✓	✓	✓	✓	✓	✓	✓
	$[M-H+Mg]^+$	<i>M+23 u</i>		✓	✓	✓	✓		
	$[M+Mg(OH)]^+$	<i>M+41 u</i>	✓	✓	✓	?	✓		✓
	$[nM+(H_2SO_4)+H]^+$	<i>M+99 u</i>	✓	?	?				
	$[M+(MgSO_4)+H]^+$	<i>M+121 u</i>	✓	✓			✓		✓
	$[M+(MgSO_4)+Mg-H]^+$	<i>M+143 u</i>		?	✓		✓		
	$[M+(MgSO_4)+Mg(OH)]^+$	<i>M+161 u</i>	✓	?	✓		✓		✓
0.1M MgSO ₄	$[M+H]^+$	<i>M+1 u</i>	✓	✓		✓	✓	✓	✓
	$[M-H+Mg]^+$	<i>M+23 u</i>		✓		✓	✓		
	$[M+Mg(OH)]^+$	<i>M+41 u</i>	✓	✓		?			
	$[nM+(H_2SO_4)+H]^+$	<i>M+99 u</i>	✓						✓
	$[M+(MgSO_4)+H]^+$	<i>M+121 u</i>		✓					
	$[M+(MgSO_4)+Mg-H]^+$	<i>M+143 u</i>		?					
	$[M+(MgSO_4)+Mg(OH)]^+$	<i>M+161 u</i>	✓	?					
1M MgSO ₄	$[M+H]^+$	<i>M+1 u</i>	✓					✓	✓
	$[M-H+Mg]^+$	<i>M+23 u</i>							
	$[M+Mg(OH)]^+$	<i>M+41 u</i>							✓
	$[nM+(H_2SO_4)+H]^+$	<i>M+99 u</i>							
	$[M+(MgSO_4)+H]^+$	<i>M+121 u</i>	✓						
	$[M+(MgSO_4)+Mg-H]^+$	<i>M+143 u</i>							
	$[M+(MgSO_4)+Mg(OH)]^+$	<i>M+161 u</i>							
Figures			S4, 4, S5	S8, S9	S10	S7	S12	S11	S6

Table 2. Characteristic detected peaks, and their respective m/z values, in cation mode for the investigated organics at 0.01M, 0.1M and 1M MgSO₄. In case of multiple species for a given concentration, the most prominent species are represented by bold checkmarks (✓). Question marks represent tentative identifications.

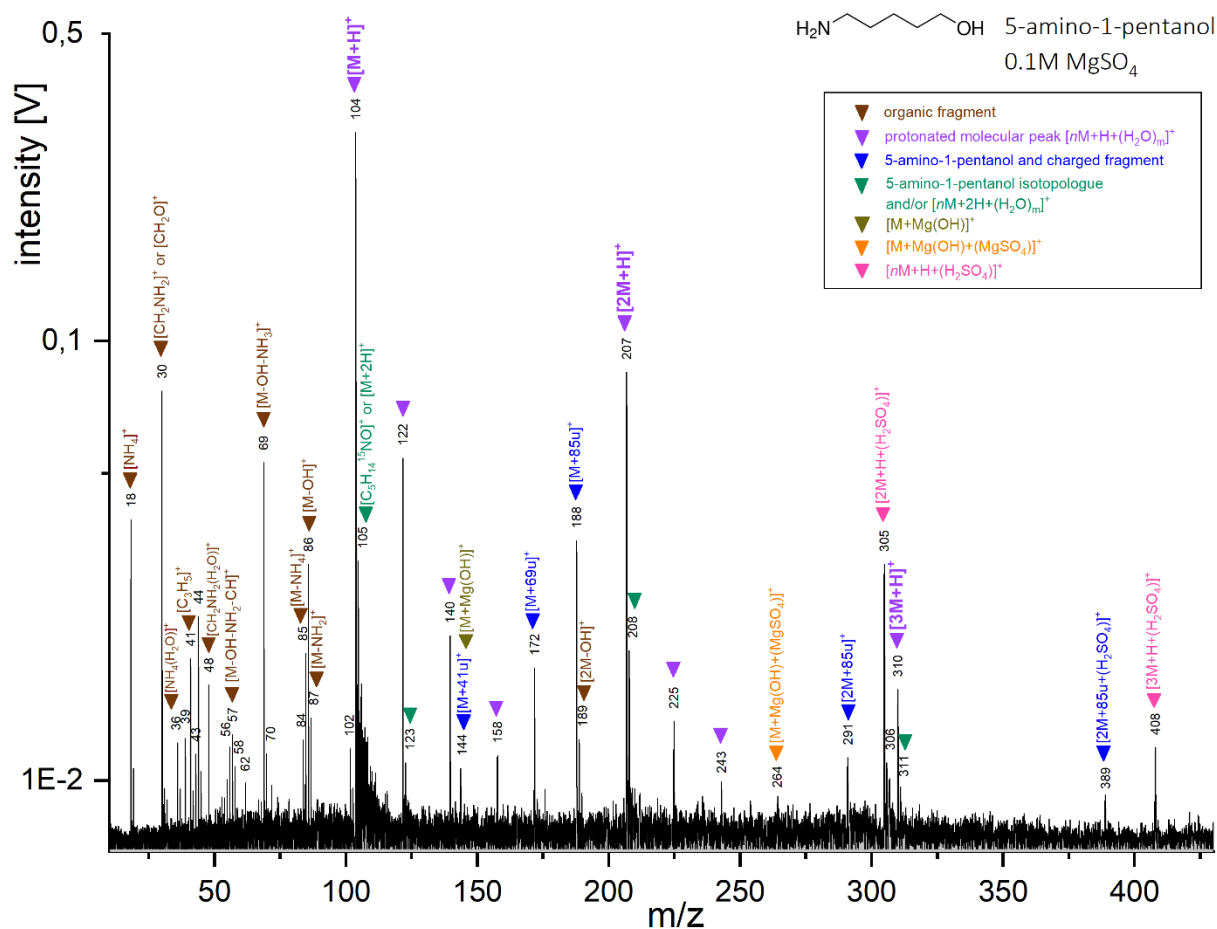


Figure 4. Baseline-corrected cation mass spectrum of 5-amino-1-pentanol (concentration 5 wt%) in 0.1M magnesium sulfate (MgSO₄), generated with a delay time of 7.0 μs.

Anion mode

In anion mode, deprotonated molecular peaks $[M-H]^-$ were detected for five organic species (acetic acid, benzoic acid, glucose, methanol and pyridine) in 0.01M MgSO₄, for three organic species (acetic acid, benzoic acid and glucose) in 0.1M MgSO₄ and only for acetic acid and benzoic acid in 1M MgSO₄ (Table 3; Figures S13-S17). Deprotonated molecular peaks have highly prominent intensities in the spectra of acetic acid and benzoic acid in all MgSO₄ concentrations (Figures S13 and S14), and in the spectra of glucose and methanol in 0.01M MgSO₄ (Figures S15 and S16).

Ionization by addition of hydrogen sulfate anion onto organic molecules was observed with the detection of $[M(\text{HSO}_4)]^-$ peaks in the spectra of 5-amino-1-pentanol, acetic acid, glucose and methanol, and $[M(\text{H}_2\text{SO}_4)(\text{HSO}_4)]^-$ peaks for 5-amino-1-pentanol and acetic acid (Table 3; Figure 4, Figures S13, S15, S16 and S18). The intensity of the $[M(\text{HSO}_4)]^-$ and $[M(\text{H}_2\text{SO}_4)(\text{HSO}_4)]^-$ peaks typically decreased with increasing MgSO_4 concentration (e.g., Figure 5 and Figure S18, Table 3).

Addition of MgSO_4 molecules onto deprotonated organic anions ($[M(\text{MgSO}_4)\text{-H}]^-$ anions) has been observed for acetic acid, benzoic acid and glucose in 0.01M MgSO_4 , and acetic acid, benzoic acid and glucose in 0.1M MgSO_4 , and acetic acid in 1M MgSO_4 (Table 3, Figures S13-S15). Adducts of magnesium sulfate and sulfate molecules onto the organic species ($[M(\text{MgSO}_4)(\text{HSO}_4)]^-$ anions) were detected for glucose in 0.01M MgSO_4 (Figure S15).

Other Mg-bearing species detected in the spectra of acetic acid in 0.01M and 0.1M MgSO_4 include $[M(\text{OH})_2+\text{Mg-H}]^-$, $[M(\text{OH})_3+\text{Mg}]^-$, $[M(\text{OH})_5+2\text{Mg}]^-$, $[2\text{M}+(\text{OH})+\text{Mg-2H}]^-$ and $[2\text{M}+(\text{OH})+(\text{MgSO}_4)+\text{Mg-2H}]^-$ anions (Figure S13). In the mass spectrum of glucose in 0.01M MgSO_4 , a peak at m/z 261 (i.e., $\text{M}+81\text{u}$) was identified as $[M(\text{HSO}_3)]^-$ anion (Figure S15). In the mass spectra of methanol in 0.1M and 1M MgSO_4 , a peak at m/z 111 (i.e., $\text{M}+79\text{u}$) was identified as $[M(\text{SO}_4)\text{-OH}]^-$ anion (Figure S19).

Peaks at m/z 124 were detected in the mass spectra of butylamine in 0.01M and 0.1M MgSO_4 (Figure S20), which correspond to $[\text{C}_2\text{H}_2(\text{H}_2\text{SO}_4)]^-$ or $[\text{CN}(\text{H}_2\text{SO}_4)]^-$, i.e., a sulfuric acid molecule added to butylamine fragments. An adduct of glucose and a charged fragment thereof ($[M(\text{C}_2\text{H}_3\text{O}_2)]^-$ at m/z 239 u) in the cation spectra of glucose in 0.01M and 0.1M MgSO_4 (Figure S15) was also identified.

			5-amino-1-pentanol <chem>NCCCCCO</chem>	Acetic acid <chem>CC(=O)O</chem>	Benzoic acid <chem>c1ccccc1C(=O)O</chem>	Butylamine <chem>CCCCN</chem>	Glucose <chem>C1C(C(C(C(O1)O)O)O)O</chem>	Methanol <chem>CO</chem>	Pyridine <chem>c1ccncc1</chem>
0.01M MgSO ₄	[M-H] ⁻	<i>M-1 u</i>		✓	✓		✓	✓	✓
	[M(HSO ₄)] ⁻	<i>M+97 u</i>	✓	✓			✓	✓	
	[M(MgSO ₄)-H] ⁻	<i>M+119 u</i>	✓	✓	✓		✓		
	[M(HSO ₄)(H ₂ SO ₄)] ⁻	<i>M+195 u</i>	✓	✓					
	[M(HSO ₄)(MgSO ₄)] ⁻	<i>M+217 u</i>					✓		
0.1M MgSO ₄	[M-H] ⁻	<i>M-1 u</i>		✓	✓		✓		
	[M(HSO ₄)] ⁻	<i>M+97 u</i>	✓	✓		✓			
	[M(MgSO ₄)-H] ⁻	<i>M+119 u</i>		✓	✓		✓		
	[M(HSO ₄)(H ₂ SO ₄)] ⁻	<i>M+195 u</i>	✓	✓					
	[M(HSO ₄)(MgSO ₄)] ⁻	<i>M+217 u</i>							
1M MgSO ₄	[M-H] ⁻	<i>M-1 u</i>		✓	✓				
	[M(HSO ₄)] ⁻	<i>M+97 u</i>						✓	
	[M(MgSO ₄)-H] ⁻	<i>M+119 u</i>		✓					
	[M(HSO ₄)(H ₂ SO ₄)] ⁻	<i>M+195 u</i>							
	[M(HSO ₄)(MgSO ₄)] ⁻	<i>M+217 u</i>							
Figures			S18, 5	S13	S14	S20	S15	S16, S19	S17

Table 3. Characteristic detected peaks, and their respective *m/z* values, in anion mode for the investigated organics at 0.01M, 0.1M and 1M MgSO₄. In case of multiple species for a given concentration, the most prominent species are represented by bold checkmarks (✓).

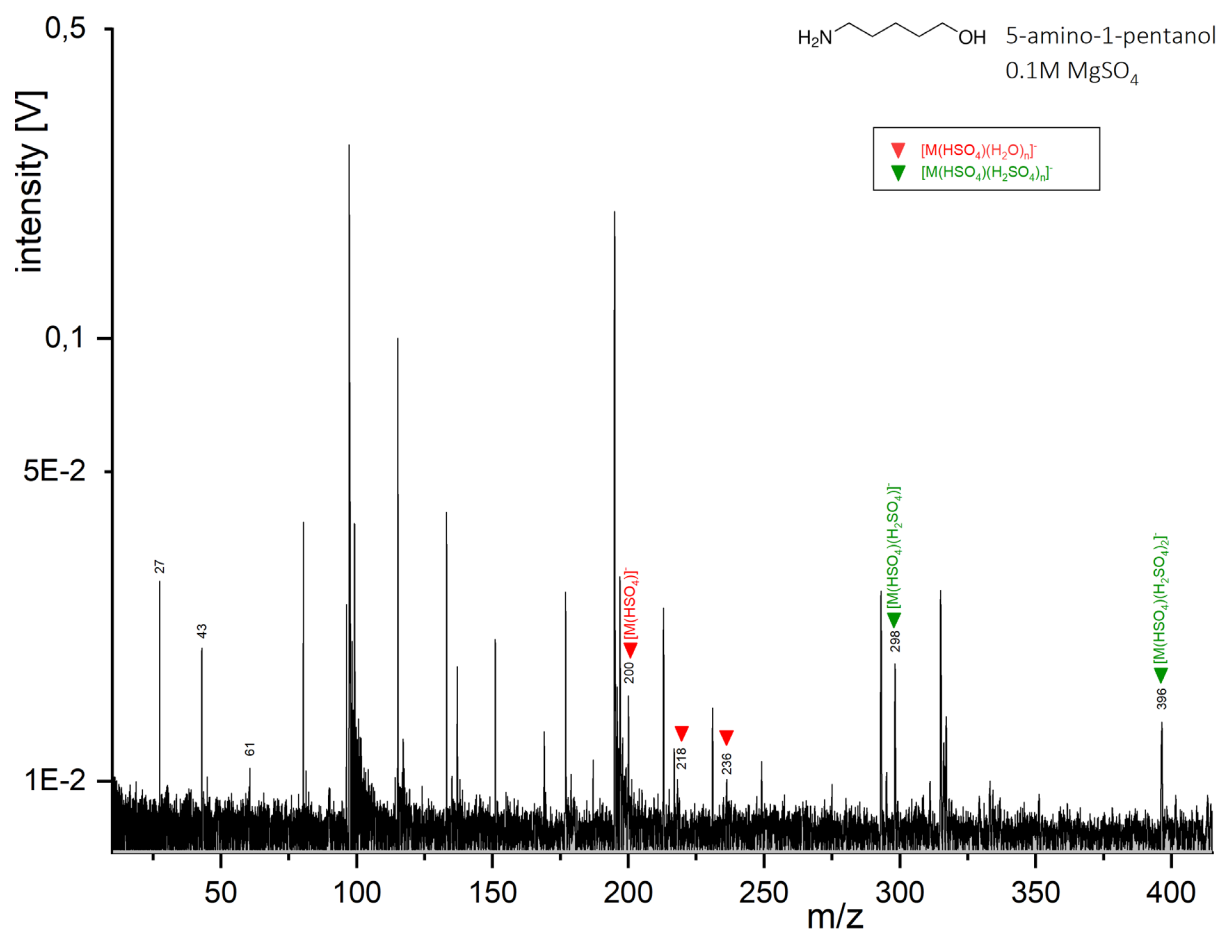


Figure 5. Baseline-corrected anion mass spectrum of 5-amino-1-pentanol (concentration 5 wt%) in 0.1M magnesium sulfate (MgSO_4), generated with a delay time of 7.3 μs . Unlabeled peaks originate exclusively from the MgSO_4 matrix.

Detection of organic fragments. In summary, the number and intensity of fragment peaks typically decreased with increasing MgSO_4 concentration in both ion modes (Table S1, Figures S3, S5). Organic fragment cations (e.g., $[\text{M-OH-NH}_3]^+$) were detected for 5-amino-1-pentanol in 0.01M, 0.1M and 1M MgSO_4 ; for acetic acid, benzoic acid, butylamine and glucose in 0.01M and 0.1M MgSO_4 ; and pyridine in the 0.01M MgSO_4 (Table S1). In anion mode, organic fragments were detected for 5-amino-1-pentanol in 0.01M and 0.1M MgSO_4 ; for acetic acid, benzoic acid, butylamine and glucose at all MgSO_4 concentrations; and pyridine in 0.01M MgSO_4 (Table S2). No fragments were detected for methanol in any of the MgSO_4 matrices investigated in neither ion mode, except a tentative fragment of methanol with sulfuric acid $[\text{M}(\text{SO}_4)\text{-OH}]^-$ or $[\text{M}(\text{SO}_3)\text{-H}]^-$ (Figure S19).

3.3. Spectra of the H_2SO_4 Background Matrix

All cation mass spectra of sulfuric acid show strong water cluster peaks $[\text{H}_3\text{O}(\text{H}_2\text{O})_n]^+$, as well as protonated sulfuric acid peaks $[\text{H}_3\text{SO}_4]^+$ and their water clusters $[\text{H}_3\text{SO}_4(\text{H}_2\text{O})_n]^+$, with n defined as $n \geq 1$ (Figures 6 and S21). In 0.01M H_2SO_4 , water cluster peaks are much higher than those from sulfuric acid (Figure S21). In 0.1M and 1M H_2SO_4 , peaks corresponding to sulfuric acid polymers $[(\text{H}_2\text{SO}_4)_n\text{+H}]^+$ and their water clusters $[(\text{H}_2\text{SO}_4)_n(\text{H}_2\text{O})_m\text{+H}]^+$ were detected (with m defined as $m \geq 1$), with n increasing with the H_2SO_4 concentration of the sample (Figure 6). Peaks at m/z 80, tentatively identified as $[\text{SO}_3]^+$ cations (see Discussion), were detected in 0.01M, 0.1M, and 1M H_2SO_4 spectra.

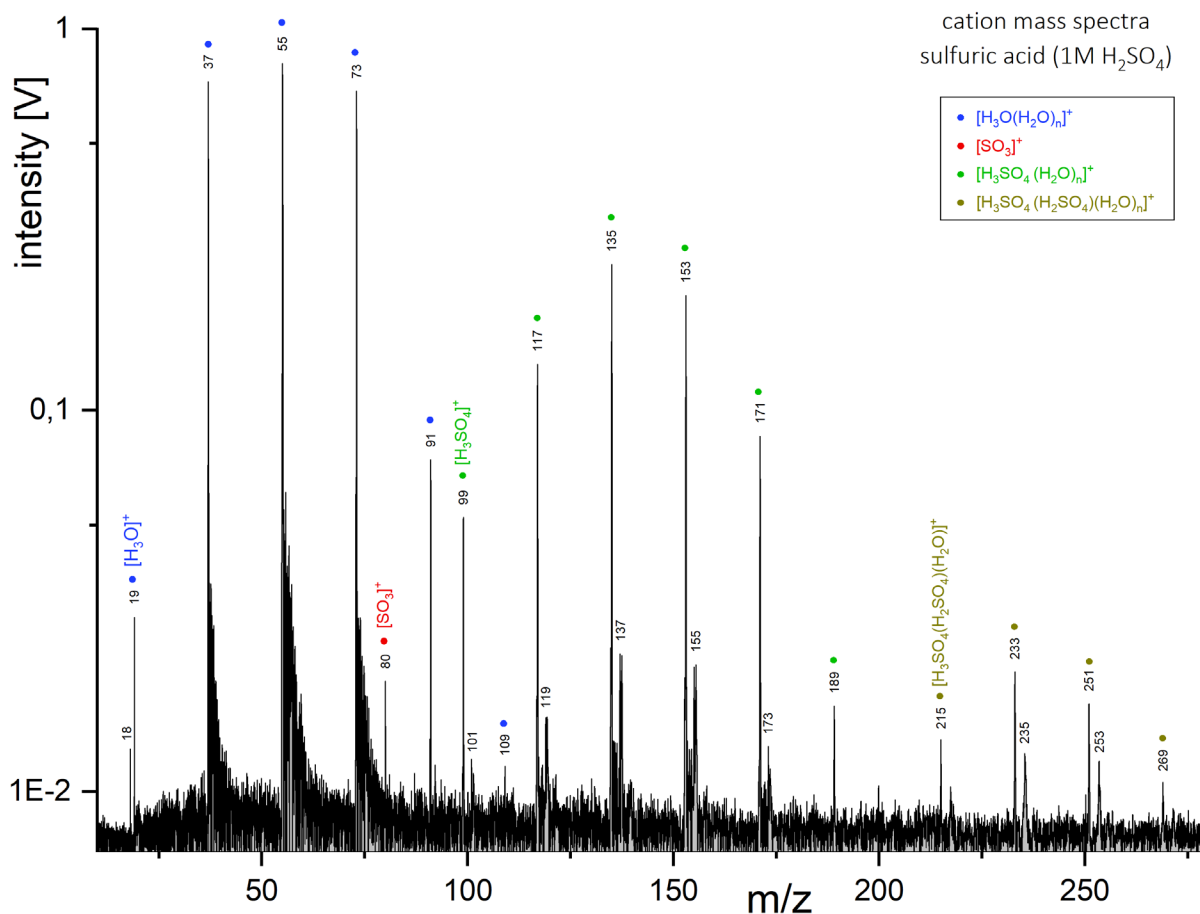


Figure 6. Baseline-corrected cation mass spectrum of sulfuric acid (H₂SO₄) at a concentration of 1M, generated with a delay time of 6.0 μs.

In anion mode, all mass spectra of sulfuric acid show prominent deprotonated sulfuric acid peaks [HSO₄]⁻, as well as sulfuric acid polymers [(HSO₄)(H₂SO₄)_n]⁻ and their respective water clusters [(HSO₄)(H₂SO₄)_n(H₂O)_m]⁻ (Figure 7 and Figure S22). The maximum number *n* of sulfuric acid molecules increased with the H₂SO₄ concentration, whereas the maximum number *m* of water clusters sulfuric acid polymers decreased with increasing H₂SO₄ concentration (Figure 7 and Figure S22). We did not detect any pure water cluster ions in any anion sulfuric acid spectrum, even at the lowest H₂SO₄ concentrations. The sulfite anion [SO₃]⁻, or the [S₂O]⁻ anion, was tentatively detected at m/z 80 in the spectra of 0.01M H₂SO₄ (Figure S22).

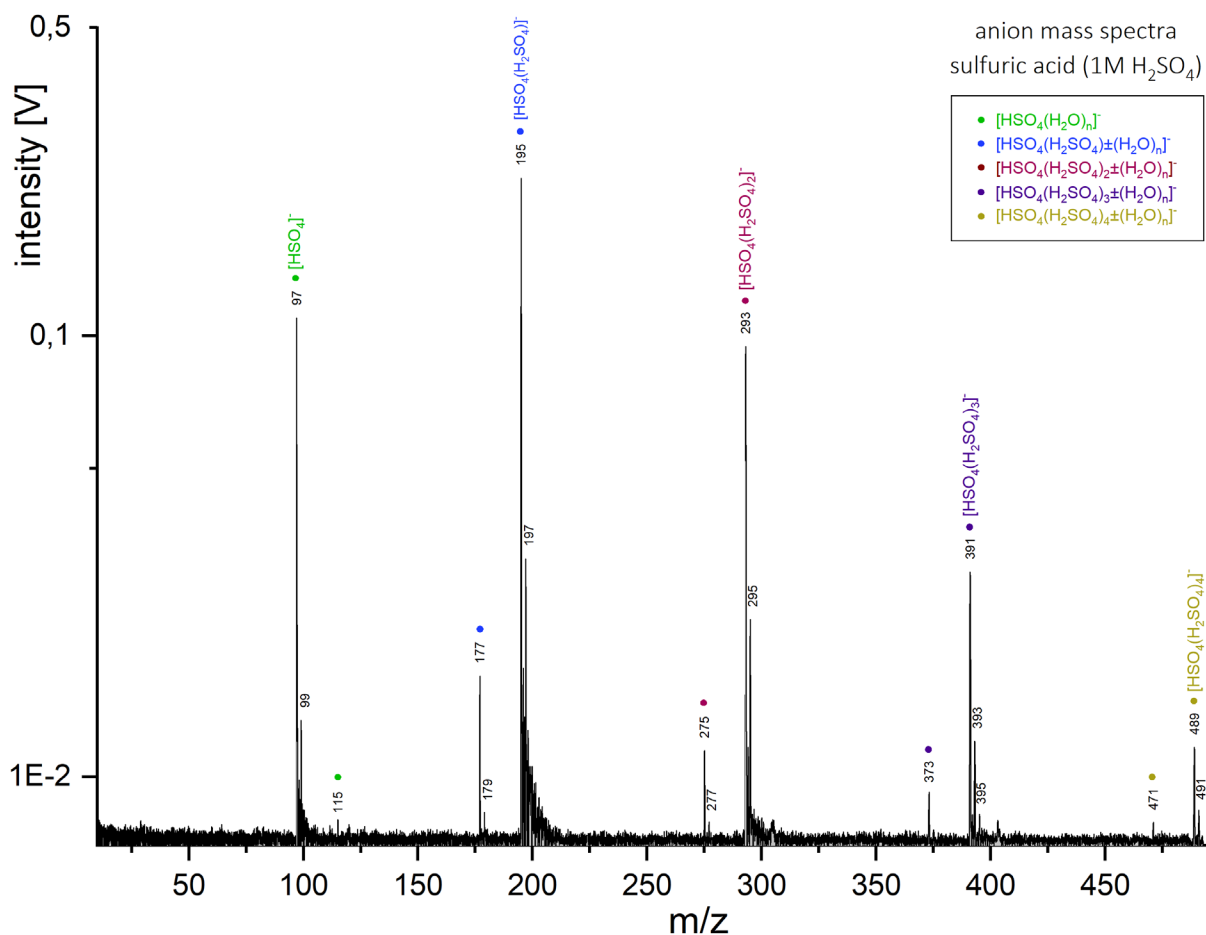


Figure 7. Baseline-corrected anion mass spectrum of sulfuric acid (H₂SO₄) at a concentration of 1M, generated with a delay time of 6.4 μ s.

3.4 Spectra of Organic Compounds in H₂SO₄-rich Matrix

In cation mode, protonated molecular peaks $[M+H]^+$ were detected for all organic species at all H₂SO₄ concentrations (Table 4). Protonated molecular peaks are the highest intensity peaks in the spectra of 5-amino-1-pentanol, butylamine, methanol and pyridine, and are highly prominent in acetic acid, benzoic acid and glucose spectra (e.g., Figure 8 and Figures S23-S30), at all H₂SO₄ concentrations. We observed the addition of H₂SO₄ molecules onto protonated organic species ($[nM+(H_2SO_4)_m+H]^+$), with the intensity and number ($m \geq 1$) of H₂SO₄ molecules increasing with the H₂SO₄ concentration of the sample (e.g., Figure 8 and Figures S23 and S24). Such $[nM+(H_2SO_4)_m+H]^+$ peaks were detected for all organic species in 0.1M and 1M H₂SO₄ (Table 4), and for four species (5-amino-1-pentanol, butylamine, glucose,

pyridine) in 0.01M H₂SO₄, and they have particularly high intensities for 5-amino-1-pentanol and butylamine (Figure 8, Figures S23, S24 and S30). The spectra of both glucose and methanol in 0.01M H₂SO₄ (Figures S28 and S29) show similar patterns of water clusters as those seen in the pure H₂SO₄ matrix spectra (Figure 6 and Figure S21).

5-amino-1-pentanol and butylamine both have much higher [2M+(H₂SO₄)+H]⁺ peaks than [M+(H₂SO₄)+H]⁺ peaks at all H₂SO₄ concentrations (Figure 8 and Figures S23, S24, and S30). This is also observed to a lower extent for acetic acid in 1M H₂SO₄ (Figure S26), pyridine in 0.01M and 0.1M H₂SO₄ (Figure S25), and methanol in 0.1M H₂SO₄.

Adducts of the organic species and charged fragments thereof ([M(M-x)]⁺ with x as a fragment of the organic species) or fragmented polymers of the organics ([nM-x]⁺ with n > 1) were detected in the cation spectra of 5-amino-1-pentanol (e.g., [M(M-OH-NH₃)]⁺; Figure 8, Figures S23 and S24), acetic acid (Figure S26), butylamine (Figure S30), and glucose (Figure S28) at all H₂SO₄ concentrations, and in the spectra of methanol in 0.1 and 1M H₂SO₄. Adducts of the organic species and charged fragments together with sulfuric acid ([M(M-x)(H₂SO₄)]⁺) were observed for 5-amino-1-pentanol in 0.1M and 1M H₂SO₄ (Figure 8 and Figure S24); butylamine, benzoic acid, and methanol in 1M H₂SO₄ (Figure S27).

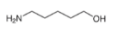
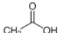
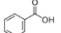
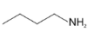
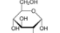
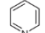
		5-amino-1-pentanol 	Acetic acid 	Benzoic acid 	Butylamine 	Glucose 	Methanol HO-CH ₃	Pyridine 
0.01M H ₂ SO ₄	[M+H] ⁺	M+1 u	✓	✓	✓	✓	✓	✓
	[M+H+(H ₂ SO ₄)] ⁺	M+99 u	✓			✓		✓
	[2M+H+(H ₂ SO ₄)] ⁺	2M+99 u	✓		✓	✓		✓
	[M+H+(H ₂ SO ₄) ₂] ⁺	M+197 u						✓
0.1M H ₂ SO ₄	[M+H] ⁺	M+1 u	✓	✓	✓	✓	✓	✓
	[M+H+(H ₂ SO ₄)] ⁺	M+99 u	✓	✓	✓	✓	✓	✓
	[2M+H+(H ₂ SO ₄)] ⁺	2M+99 u	✓		✓			✓
	[M+H+(H ₂ SO ₄) ₂] ⁺	M+197 u				✓		
1M H ₂ SO ₄	[M+H] ⁺	M+1 u	✓	✓	✓	✓	✓	✓
	[M+H+(H ₂ SO ₄)] ⁺	M+99 u	✓	✓	✓	✓	✓	✓
	[2M+H+(H ₂ SO ₄)] ⁺	2M+99 u	✓	✓	✓	✓	✓	✓
	[M+H+(H ₂ SO ₄) ₂] ⁺	M+197 u	✓	✓	✓	✓		
Figures		S23, S24, 8	S26	S27	S30	S28	S29	S25

Table 4. Characteristic detected peaks, and their respective m/z values, in cation mode for the investigated organics at 0.01M, 0.1M and 1M H_2SO_4 . In case of multiple species for a given concentration, the most prominent species are represented by bold checkmarks (✓).

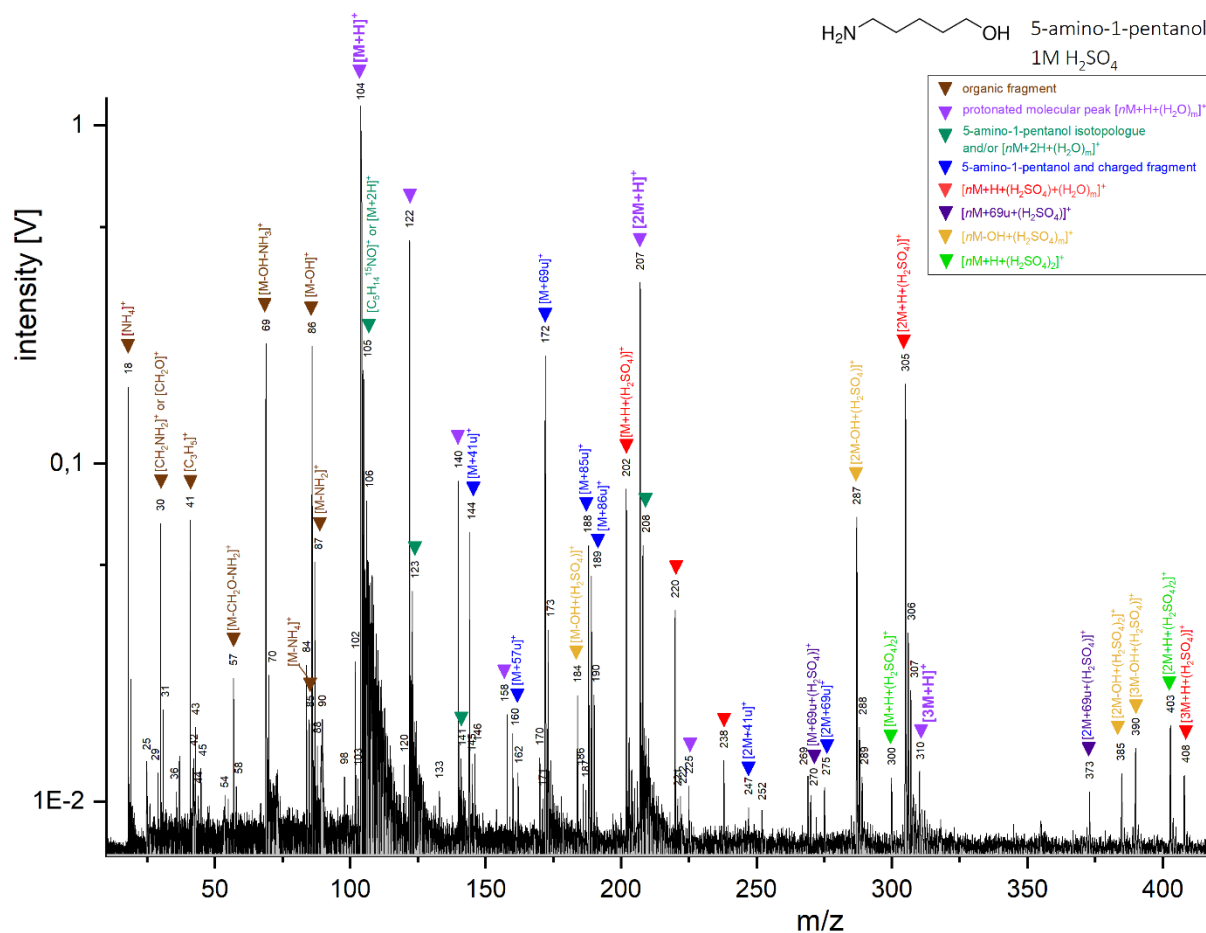


Figure 8. Baseline-corrected cation mass spectrum of 5-amino-1-pentanol (concentration 5 wt%) in 1M sulfuric acid (H_2SO_4), generated with a delay time of 6.9 μs .

In anion mode, deprotonated molecular peaks $[M-H]^-$ were detected for three organic species (5-amino-1-pentanol, acetic acid and benzoic acid; Table 5, Figures S31-S33). A higher number of organic species can be detected by their $[M(HSO_4)]^-$ peaks (Table 5): in 0.01M and 0.1M H_2SO_4 , all organics except butylamine and pyridine; in 1M H_2SO_4 , glucose and tentatively acetic acid. $[M(H_2SO_4)_n(HSO_4)]^-$ peaks were detected for 5-amino-1-pentanol,

acetic acid, glucose and methanol in 0.01M and 0.1M H₂SO₄ (Table 5, Figures S14-S36), and for 5-amino-1-pentanol (Figure 4) and methanol in 1M H₂SO₄. The observable number, *n*, of polymers of sulfuric acid [M(H₂SO₄)_{*n*}(HSO₄)]⁻ increased with the H₂SO₄ concentration (e.g., Figure 9 and Figure S31). [M(HSO₄)(SO₃)]⁻ peaks have been detected for glucose in 0.01M and 0.1M H₂SO₄ (Figure S35); and for 5-amino-1-pentanol and glucose in 1M H₂SO₄ (Figure 9).

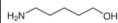
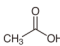
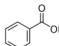
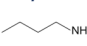
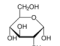
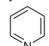
			5-amino-1-pentanol 	Acetic acid 	Benzoic acid 	Butylamine 	Glucose 	Methanol HO—CH ₃	Pyridine 
0.01M H₂SO₄	[M-H] ⁻	<i>M-1 u</i>	✓	✓	✓				
	[M(HSO ₄)] ⁻	<i>M+97 u</i>	✓	✓	✓		✓	✓	
	[M(H ₂ SO ₄) _{<i>n</i>} (HSO ₄)] ⁻	<i>M+195 u</i>	✓	✓		✓	✓		
0.1M H₂SO₄	[M-H] ⁻	<i>M-1 u</i>							
	[M(HSO ₄)] ⁻	<i>M+97 u</i>	✓	✓	✓		✓	✓	
	[M(H ₂ SO ₄) _{<i>n</i>} (HSO ₄)] ⁻	<i>M+195 u</i>	✓	✓		✓	✓	✓	
1M H₂SO₄	[M-H] ⁻	<i>M-1 u</i>							
	[M(HSO ₄)] ⁻	<i>M+97 u</i>		?			✓		
	[M(H ₂ SO ₄) _{<i>n</i>} (HSO ₄)] ⁻	<i>M+195 u</i>	✓			✓	?	✓	
Figures			S31, S34, 9	S32	S33	S37	S35	S36	

Table 5. Characteristic detected peaks, and their respective *m/z* values, in anion mode for the investigated organics at 0.01M, 0.1M and 1M H₂SO₄. Question marks represent tentative identifications. In case of multiple species for a given concentration, the most prominent species are represented by bold checkmarks (✓).

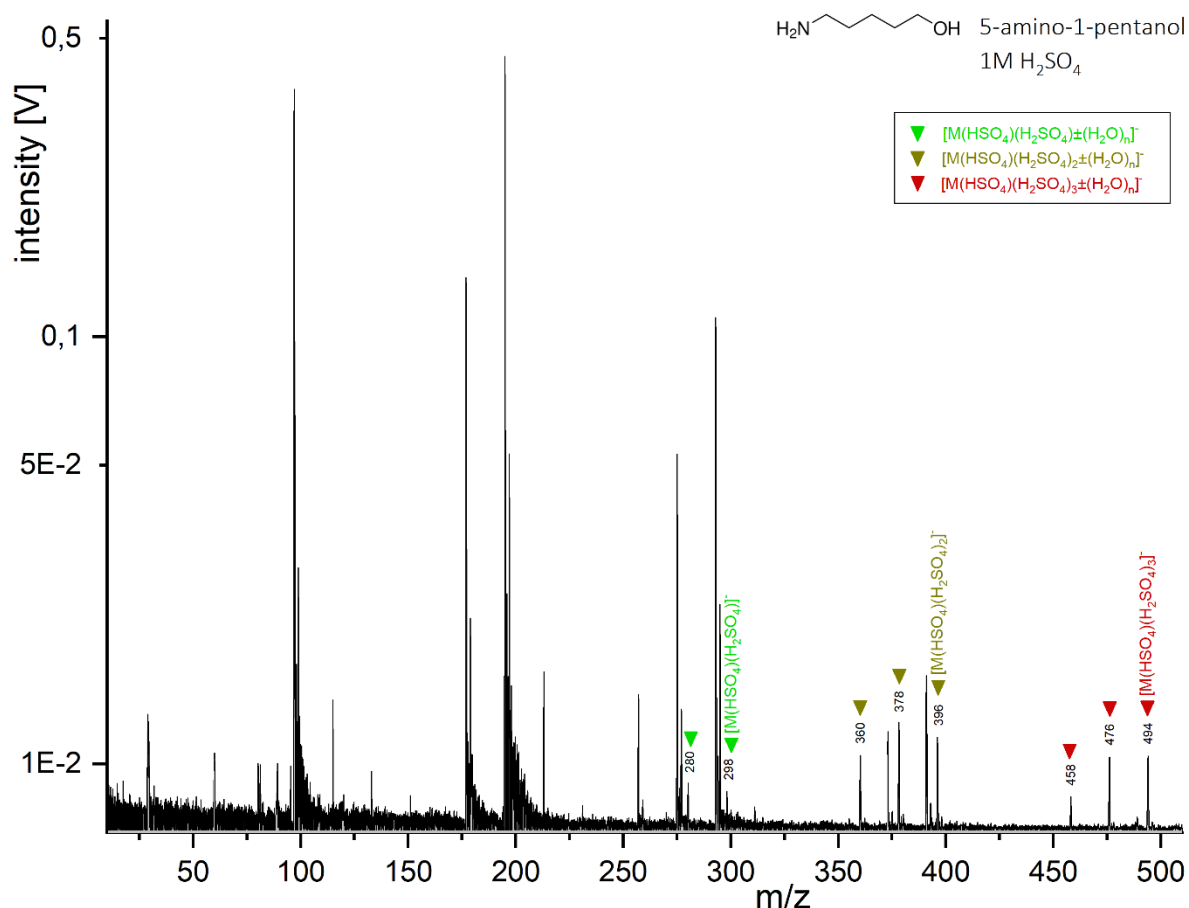


Figure 9. Baseline-corrected anion mass spectrum of 5-amino-1-pentanol (concentration 5 wt%) in 1M sulfuric acid (H_2SO_4), generated with a delay time of 6.9 μs . Unlabeled peaks originate exclusively from the H_2SO_4 matrix.

Detection of organic fragments. Organic fragment cations were detected for 5-amino-1-pentanol, acetic acid, benzoic acid, butylamine and glucose at all H_2SO_4 concentrations, and for methanol and pyridine in 1M H_2SO_4 (Tables S3). In contrast to the observations in the NaCl and MgSO_4 matrices, both the intensity and number of detected cationic fragments is usually unchanged or even increase with the H_2SO_4 concentration (e.g., Figure 8, Figures S23 and S24; Table S1). In anion mode, organic fragments were only detected for 5-amino-1-pentanol and butylamine in 0.01M H_2SO_4 (Table S2).

3.5 Summary of General Trends

Our results show that organic species can be detected in ice grains rich in magnesium sulfate and sulfuric acid, due to the formation of molecular ions, fragment ions and a range of adducts with Mg^{2+} , OH^- , HSO_4^- ions, and MgSO_4 and H_2SO_4 molecules. The mass spectral appearance of the organics fundamentally changes depending on the matrix (MgSO_4 or H_2SO_4) and the matrix concentration. Similar to NaCl matrices, strong suppression effects by the salt^{1,68} were observed in MgSO_4 matrices in both ion modes, i.e., the absolute number and intensities of organic-related peaks decrease with increasing MgSO_4 concentration (Tables 2, 3, Figure 5, Figures S4, S5, S18). Suppression effects were also observed in H_2SO_4 matrices in anion mode, but to a lower extent than in MgSO_4 matrices (Table 5, Figure 9, Figures S31, S34). However, no suppression effects were observed in H_2SO_4 matrices in cation mode. The intensity of suppression effects was characterized for organics in NaCl , MgSO_4 and H_2SO_4 matrices in both ion modes (Table 6). Detection limits were established in pure water matrix (Table 6) for the (de)protonated molecular peaks of all organic species in the most sensitive ion mode. Detection limits are estimated to be similar in pure water and in H_2SO_4 matrices for organics in cation mode.

	LOD in pure H ₂ O matrix in best ion mode	NaCl		MgSO ₄		H ₂ SO ₄				
		Best ion mode	suppression effects		Best ion mode	suppression effects		Best ion mode	suppression effects	
			cation mode	anion mode		cation mode	anion mode		cation mode	anion mode
5-amino-1-pentanol	1 ppb [+] (10 ⁻⁷ wt%)	+	Low: 2 orders of magnitude	High: >2 orders of magnitude	+	Low: 1 order of magnitude	High: >2 orders of magnitude	+	None	Intermediate: 1 order of magnitude
acetic acid	<1 ppb* [-] (< 10 ⁻⁷ wt%)	-	Intermediate: 2 orders of magnitude	Low: 1 order of magnitude	-	High: >2 orders of magnitude	Low: 1 order of magnitude	+	None	Intermediate: 2 orders of magnitude
benzoic acid	1 ppb [-] (10 ⁻⁷ wt%)	-	High: >2 orders of magnitude	Low: 1 orders of magnitude	-	High: >2 orders of magnitude	Low: 1 order of magnitude	+	None	High: >2 orders of magnitude
butylamine	<1 ppb* [+] (< 10 ⁻⁷ wt%)	+	Intermediate: 2 orders of magnitude	High: >2 orders of magnitude	+	High: >2 orders of magnitude	Intermediate: <1 order of magnitude	+	None	Intermediate: <1 order of magnitude
glucose	100 ppm [+] (10 ⁻² wt%)	+	Low: 1 order of magnitude	High: >2 orders of magnitude	-	High: >2 orders of magnitude	Intermediate: 1 orders of magnitude	+	None	Intermediate: 1 order of magnitude
methanol	500 ppm [+] (5×10 ⁻² wt%)	+	Intermediate: 1 order of magnitude	High: >2 orders of magnitude	+	Low: 1 order of magnitude	Intermediate: <1 order of magnitude	+	None	Intermediate: 1 order of magnitude
pyridine	1 ppb [+] (10 ⁻⁷ wt%)	+	Intermediate: 2 orders of magnitude	High: >3 orders of magnitude	+	None	High: >3 orders of magnitude	+	None	High: >3 orders of magnitude

* the exact LOD of acetic acid and butylamine in water matrix was not determined, but this value is lower than 1 ppb.

Table 6. Limits of detection (LOD) of (de)protonated molecular peaks of the organic species in pure water matrix with LILBID, and the estimated intensities of suppression effects for all organic species in the different matrices (NaCl, MgSO₄, H₂SO₄). The (+) or (-) in the first column gathering the LODs indicate the ion mode in which the LOD was measured – cation mode for (+) or anion mode for (-). No suppression effects were observed for organics in H₂SO₄ matrices in cation mode, and pyridine in MgSO₄ matrix. For all other matrices, the suppression effects are considered “low” when organics’ (de)protonated molecular peaks were detected in all matrix concentrations (from 0.01M to 1M); “intermediate” when any organic ions (including organic fragments and clusters) were detected in all matrix concentrations; and “high” when no organic ions were detected at the highest matrix concentration of 1M. Additionally, the strength of the suppression effects was quantified - with order of magnitude accuracy - by comparing the ion abundances of the highest organic-bearing ion between the spectra of organics in the pure water matrix, and in the NaCl, MgSO₄, or H₂SO₄ matrices at 1M concentration

Cation mode is generally more sensitive than anion mode to organics in MgSO₄ solutions (Tables 2 and 3), especially for butylamine and pyridine – two species for which the sensitivity is very low in anion mode. However, acetic acid and benzoic acid in MgSO₄ matrices are more easily detected in anion mode than cation mode. Cation mode is preferred over anion mode for the detection of all organic species in H₂SO₄ matrices because organic species can be unambiguously detected via protonated molecular peaks even at the highest sulfuric acid concentrations (Tables 4).

In both MgSO₄ and H₂SO₄ matrices, interactions of the organic species with sulfates lead to the detection of [M(HSO₄)]⁻ anions for four organic species (5-amino-1-pentanol, acetic acid, glucose and methanol). [M(HSO₄)]⁻ anions were also detected in the spectra of benzoic acid only in H₂SO₄ solutions. These anion peaks are suppressed with increasing matrix concentration in both MgSO₄ and H₂SO₄ matrices. [M(H₂SO₄)_n(HSO₄)]⁻ anions (with $n \geq 1$) were detected in both MgSO₄ and H₂SO₄ matrices: for 5-amino-1-pentanol and acetic acid in MgSO₄ matrices, and all organics except benzoic acid and pyridine in H₂SO₄ matrices. The maximum number, n , of (H₂SO₄) molecules in [M(H₂SO₄)_n(HSO₄)]⁻ peaks typically increased with increasing matrix concentration.

Adducts of organics with H₂SO₄ molecules were observed in both matrices and in both ion modes, although more frequently in H₂SO₄ matrices (e.g., [M(H₂SO₄)+H]⁺ peaks were observed for one, and tentatively for two, organic species in MgSO₄ matrices, and for all organic species in H₂SO₄ matrices). In H₂SO₄ matrices, the intensities and number of [M(H₂SO₄)_n+H]⁺ peaks typically increased with increasing H₂SO₄ concentrations, whereas these peaks are suppressed in MgSO₄ matrices with increasing MgSO₄ concentration. We observe [n M+(H₂SO₄)_m+H]⁺ peaks for all species at H₂SO₄ concentrations ≥ 0.1 M, and for most species at an H₂SO₄ concentration of 0.01M. The [n M(H₂SO₄)_m+H]⁺ peaks are especially prominent for basic species (i.e., 5-amino-1-pentanol and butylamine). In MgSO₄ matrices,

adducts of MgSO₄ molecules with organic ions were observed in both ion modes, with the detection of [M(MgSO₄)+H]⁺, [M(MgSO₄)-H]⁻, [M(MgSO₄)+Mg-H]⁺ and [M(MgSO₄)(OH)+Mg]⁺ ions.

Generally, a lower degree of fragmentation was observed in NaCl matrices as compared to MgSO₄ and H₂SO₄ matrices in cation mode for most species (i.e., 5-amino-1-pentanol, acetic acid, benzoic acid, glucose, pyridine). The absolute number and intensities of fragment peaks are higher in cation mode than anion mode for all organic species in all three matrices.

Comparing organic fragments detected in sulfate matrices of this work (Tables S1, S2) with fragments detected in NaCl matrices², the following trends can be established:

- **5-amino-1-pentanol:** the type and abundance of cationic fragments of 5-amino-1-pentanol detected in MgSO₄ and H₂SO₄ matrices were roughly similar in both matrices, but a much smaller number of fragments were detected in NaCl matrices.
- **carboxylic acids:** highly prominent [M-OH]⁺ fragments were detected in the mass spectra of both acetic acid and benzoic acid in MgSO₄ and H₂SO₄ matrices (at all matrix concentrations), whereas in NaCl matrices, they were detected only at low NaCl concentrations and at much lower intensities. Such peaks were also very prominent in the cation mass spectra of acetic acid and benzoic acid in pure water matrices².
 - **Acetic acid:** more cationic fragments of acetic acid were detected in MgSO₄ matrices than in H₂SO₄ matrices, and very few in NaCl matrices. In the anion spectra, [CH₃]⁻ fragments were detected in both MgSO₄ and NaCl matrices, but no fragments were detected in H₂SO₄ matrices.
 - **Benzoic acid:** more cationic fragments of benzoic acid were detected in H₂SO₄ matrices than in MgSO₄ matrices, and very few in NaCl matrices. In

anion mode, deprotonated benzene was detected in both MgSO₄ and NaCl matrices, but no benzoic acid fragments were detected in H₂SO₄ matrices.

- **Butylamine:** a decreasing trend with matrix composition was found in the number and intensities of cationic fragments of butylamine: MgSO₄ > H₂SO₄ > NaCl. In anion mode, only one anionic fragment was detected in H₂SO₄ matrices, whereas many more anionic fragments were detected in MgSO₄ and NaCl matrices. Very prominent fragment peaks (e.g., [C₂H₂]⁻ or [CN]⁻ at m/z 26; Figure S20) were detected in the anion spectra of butylamine in MgSO₄ matrices at all MgSO₄ concentrations.
- **Glucose:** many cationic fragments of glucose, but no anionic fragments, were detected in H₂SO₄ matrices. Fewer cationic fragments were detected in MgSO₄ matrices than H₂SO₄ matrices, and even less in NaCl matrices. Anionic fragments were detected in MgSO₄ and NaCl matrices, with more fragments and at higher intensities in NaCl matrices.
- **Methanol:** the only methanol fragment detected was [CH₃]⁺ in the 1M H₂SO₄ matrix, and together with sulfate [CH₃(SO₄)]⁻ in 0.1M and 1M MgSO₄.
- **Pyridine:** small fragment peaks of pyridine were detected in the 1M H₂SO₄ matrix and in 0.01M MgSO₄ matrix in cation mode, and in the 0.01M MgSO₄ matrix in anion mode whereas no fragments were detected in the NaCl matrices.

4 Discussion

Suppression effects. Suppression effects are described as the decrease in the mass spectrometric response of an analyte due to matrix effects⁶⁹. In the H₂SO₄ matrix, no ionization suppression effects occurred in cation mode (because the only cation species sulfuric acid releases in water is H⁺), whereas suppression effects were observed in anion mode. The mass

spectra of organics in MgSO₄ matrices show suppression effects with increasing matrix concentration, a phenomenon frequently seen for the detection of analytes in salt-rich matrices^{1,68}. This effect (in MgSO₄ matrices) is similar or stronger than that seen for the same organic compounds in NaCl matrices². While detection limits can typically drop by orders of magnitude with high concentrations of salts, this effect is strongly compound-dependent and was mild for some organic species (e.g., for 5-amino-1-pentanol in 1M MgSO₄ as seen in Figure S5).

The origins and mechanisms of ionization suppression in mass spectrometry are poorly understood. King et al.⁷⁰ showed that the presence of nonvolatile solutes is the main cause of ionization suppression in electrospray ionization (ESI) due to induced changes in the droplet solution properties. They suggested that nonvolatile materials inhibit the formation of small droplets and therefore the release of analytes into the gas phase. In the LILBID setup, the analyte is converted from the liquid water beam into gas phase ions, so coprecipitation of organic molecules (before the formation of gaseous ions) with nonvolatile sample components could be an efficient mechanism of ionization suppression. Gas phase reactions, such as acid-base neutralization or charge transfer to another gas phase species, could also lead to a loss of charge in the total ions created in the LILBID experiments. Both explanations are consistent with the fact that suppression effects are compound-dependent (i.e., they have different intensities for different organic species in a given matrix).

Fragmentation of the organic species. In MgSO₄ matrices, the number and the intensities of organic fragment peaks typically decrease with increasing MgSO₄ concentration in both ion modes (Table S1, Figures S3, S5), a trend similar to that observed in NaCl matrices². This result reinforces our hypotheses that high salinity matrices might provoke the suppression of the fragmentation process (i.e., adducts of organics and salts are more stable than the pure organics) or the neutralization of charged fragments (or neutral fragments are produced).

Sulfuric acid does not appear to inhibit the formation of cationic fragments since (1) we detected a high number of cationic fragments (Table S1), which in some cases increased with increasing H₂SO₄ concentration (2) almost all cationic fragments detected in water matrices were also detected in H₂SO₄ matrices. However, anionic fragments were only detected via infrequent, low amplitude, peaks and at low H₂SO₄ concentrations, probably due to a lower sensitivity to organic species with increasing H₂SO₄ concentration.

Comparing the organic fragments detected in MgSO₄, H₂SO₄ and NaCl matrices (Section 3.5), we observe a wide diversity of fragments varying with the matrix's nature and concentration. Each matrix induced different fragmentation patterns, e.g., the cation spectra of organics in NaCl matrices show fewer fragments compared to MgSO₄ and H₂SO₄ matrices and entirely inhibited fragmentation of hydroxyl groups in carboxylic acids (a typical cleavage of carboxylic acids; section 3.5). Fragment peaks are also subject to suppression effects with increasing salt concentration in MgSO₄ and NaCl matrices. This variability of fragmentation patterns might be due to differences in the energetics of the fragmentation mechanisms induced by the varying matrix. For SUDA's analysis, many other factors than the matrix's composition will influence the level of fragmentation of organics embedded in ice grains, such as the impact velocity, the pH of the ice matrix and the spatial distribution of the organic species inside the ice grain^{e.g.,71,72}. Schulze et al.⁷² showed that in extreme saline ice (>1M), salting-out effects (i.e., a decrease in solubility at high salt concentrations leading to phase separation of organics, salts, and water) shield organic species from the impact energy, therefore further limiting fragmentation by alteration of the ice's mechanical behavior.

We detected [M+M-x]⁺ and [M+M-x]⁻ species where *x* is a fragment of the organic species (e.g., [2M-OH-NH₃]⁺; Figure 4). They might form by fragmentation of an organic polymer rather than by addition of a charged fragment onto a neutral organic molecule, because we

observe fragmented polymers (e.g., $[(3M-OH-NH_3)]^+$ in 5-amino-1-pentanol in 0.01M $MgSO_4$ matrix; Figure S4) but no addition of several charged fragments onto an organic molecule.

We observed oxygen-carrying fragment ions in the spectra of 5-amino-1-pentanol, acetic acid, benzoic acid and glucose, and nitrogen-carrying fragment ions in the spectra of 5-amino-1-pentanol, butylamine and pyridine. Khawaja et al.⁷³ measured a range of aldehydes and ketones with the LILBID technique, and showed that oxygen-carrying fragment ions (e.g., $[CHO]^+$, $[CH_3O]^+$, $[C_2H_3O]^+$, $[C_2H_5O]^+$...) were also typically produced. Some fragments were observed in $MgSO_4$ and/or H_2SO_4 matrices, but not in the spectra of the organic species in pure water (e.g., $[C_2H_4N]^+$ was observed only for butylamine in $MgSO_4$ matrices, $[NH_4]^+$ for pyridine in 1M H_2SO_4 matrix, $[C_3H_3]^+$ or $[HCCN]^+$ for butylamine in H_2SO_4 matrices, $[CHO]^+$ for acetic acid in $MgSO_4$ matrices; Tables S1, S2). These species may therefore indicate that different fragmentation patterns appear due to compositional differences in the matrix; or they might be products of interactions of organic fragments with matrix compounds.

In mass spectrometry experiments, organic fragments can interact with ions from the matrix, thus forming for example sodiated or chlorinated fragments in NaCl matrices^{e.g.,74}. Although we did not detect sodiated or chlorinated fragments with LILBID (potentially because of the suppression of fragmentation processes or the neutralization of charged fragments²), we detected a few species formed by the interaction of organic fragments with ions from the $MgSO_4$ or H_2SO_4 matrix:

- a species consisting of a charged butylamine fragment and a sulfuric acid molecule ($[C_2H_2(H_2SO_4)]^-$ or $[CN(H_2SO_4)]^-$ at m/z 124) in the anion spectra of butylamine in 0.01 and 0.1M $MgSO_4$ matrices (Figure S20)
- $[nM+(H_2SO_4)_m-OH]^+$ and $[2M+(H_2SO_4)_m-OH-NH_3]^+$ cations in the spectra of 5-amino-1-pentanol in 1M H_2SO_4 matrix (Figure 8)

- $[\text{C}_2\text{H}_4\text{N}+\text{Mg}+\text{SO}_3]^-$ anions in the spectra of 5-amino-1-pentanol in 0.01M H_2SO_4 matrix (Figure S31)
- a fragment of methanol with sulfuric acid $[\text{M}(\text{SO}_4)\text{-OH}]^-$ in MgSO_4 matrix.

Ion formation from organic/matrix interaction. In MgSO_4 solutions, we observed the addition of Mg^{2+} cations onto both deprotonated organic species ($[\text{M-H}+\text{Mg}]^+$) and together with OH^- groups (e.g., $[\text{M}(\text{OH})_2+3\text{Mg-H}]^+$, $[\text{M}(\text{OH})_3+2\text{Mg}]^+$, $[\text{M}(\text{OH})_2+\text{Mg}+\text{H}]^+ \dots$). Magnesium adducts including $[\text{M}+\text{Mg-H}]^+$ cations have previously been observed by Han et al.⁷⁵ with electrospray ionization (ESI) mass spectrometry. As the LILBID ionization method tends to produce singly charged ions, and magnesium (Mg^{2+}) and sodium (Na^+) ions have different charges, the organic cations formed in MgSO_4 matrices are different from the species observed in NaCl matrices, where sodium adducts form with organic molecules via sodiation processes^{e.g.,1,2,76}. The replacement of structural elements by Na^+ cations (i.e., sodiation) seems to be more efficient than by Mg^{2+} cations, as protonated organic species typically dominate the cation spectra of MgSO_4 matrices whereas sodiated cations typically dominate in NaCl matrices^{1,2}. In organic molecules, it is easier to replace H^+ with Na^+ than with Mg^{2+} because Na^+ and H^+ have the same charge. Additionally, the larger size of Mg^{2+} ions compared to Na^+ slows down the attachment to organic molecules by steric hindrance.

In anion mode, we observe the addition of hydrogen sulfate anions HSO_4^- to organic species (i.e., bisulfate adducts $[\text{M}(\text{HSO}_4)]^-$) in both MgSO_4 and H_2SO_4 solutions. Bisulfate adducts $[\text{M}(\text{HSO}_4)]^-$ were previously observed by other mass spectrometry methods e.g., with Matrix Assisted Laser Desorption Ionization (MALDI)⁷⁷ and with ESI-MS⁷⁸. The formation of bisulfate adducts is comparable to the chlorination of organics (i.e., addition of a chloride anion) in NaCl matrices^{2,79,80}.

In both ion modes, we observed the addition of MgSO_4 and H_2SO_4 molecules to organic ions in MgSO_4 matrices and the addition of H_2SO_4 molecules in H_2SO_4 matrices. Addition of H_2SO_4 molecules is therefore a common characteristic pattern in sulfate-rich matrices. The addition of MgSO_4 molecules onto organic cations was observed for all organic species except butylamine and methanol, suggesting that linear molecules having few functional groups might be less prone to the addition of MgSO_4 molecules. The observed addition of NaCl and NaOH molecules in NaCl matrices^{1,2} is consistent with these mechanisms. The number of added H_2SO_4 and NaCl molecules often increased with increasing matrix concentration. Attachment of sulfuric acid molecules onto peptides and proteins have been previously reported by using ESI-MS⁸¹, together with a decrease of the mass spectrometric signal.

In the cation spectra of the sulfuric acid matrix without organics (Figures 6, S21), cations at m/z 80 were identified as $[\text{SO}_3]^+$ as seen in the electron ionization spectra retrieved from the National Institute of Standards and Technology (NIST). The $[\text{SO}_3]^+$ cation can form by the loss of water from H_2SO_4 . Although sulfuric acid is intrinsically different from salts, mass spectral similarities can be found in the spectra of organics in MgSO_4 and H_2SO_4 matrices. This is due to the presence of sulfates in both MgSO_4 and H_2SO_4 matrices, therefore inducing the formation of similar species in both matrices.

In the cation mass spectra of 5-amino-1-pentanol and butylamine in H_2SO_4 matrices (Figures 8, S23, S24, S30), and to a lesser extent in the spectra of 5-amino-1-pentanol in the MgSO_4 matrix (Figures 4, S4), we observe $[2\text{M}+(\text{H}_2\text{SO}_4)+\text{H}]^+$ in higher abundance than $[\text{M}+(\text{H}_2\text{SO}_4)+\text{H}]^+$. As shown in Figure 10, this could be because $[2\text{M}+(\text{H}_2\text{SO}_4)+\text{H}]^+$ cations preferentially form as $[2(\text{M}+\text{H})+(\text{SO}_4)+\text{H}]^+$ cations (i.e., two protonated organic molecules interact with one SO_4^{2-} anion, and the adduct thus formed is protonated), and $[\text{M}+(\text{H}_2\text{SO}_4)+\text{H}]^+$ cations are rather formed as $[(\text{M}+\text{H})+(\text{HSO}_4)+\text{H}]^+$ cations (i.e., a protonated organic molecule interacts with HSO_4^- , and the adduct thus formed is protonated). This formation mechanism is

explained by the dissociation of sulfuric acid in water into different ions including hydrogen sulfate HSO_4^- and sulfate SO_4^{2-} : the sulfate ion has two negative charges making it more likely to interact with two other positively charged molecules. If sulfuric acid is predominantly present as SO_4^{2-} (i.e., at high pH), then $[2(\text{M}+\text{H})+(\text{SO}_4)+\text{H}]^+$ cations are more likely to form than $[(\text{M}+\text{H})+(\text{HSO}_4)+\text{H}]^+$ cations. This mass spectral pattern was observed for the two most basic species we measured (i.e., 5-amino-1-pentanol and butylamine; Table 1).

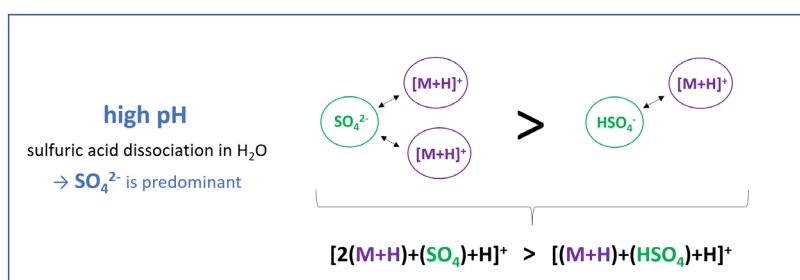


Figure 10. Possible interaction of basic organic species with sulfate ions, explaining the higher intensities of $[2(\text{M}+\text{H})+(\text{SO}_4)+\text{H}]^+$ cations as compared to $[(\text{M}+\text{H})+(\text{HSO}_4)+\text{H}]^+$ cations.

The differences in sensitivity to the organics between different matrices is primarily due to the organics' properties (e.g., pH, the presence of functional groups). The molar concentration of the organic species in solution can also play a role (since the organic species were investigated at similar weight percentages but consequently at different molar concentrations; Table 1), but no direct correlation was observed between the sensitivity to an organic species and its molar concentration in solution. This suggests that the difference in molecular densities in the ionization region of the LILBID only plays a minor role in the sensitivity to the organics.

Liquid phase reactions. Liquid phase reactions can occur in solution when mixing organic species with salts or sulfuric acid. Reactions involving high concentrations of sulfuric acid played a significant role in our experiments, e.g., amines participated in acid-base reactions with sulfuric acid in solution and were partially precipitated as salts in the samples of butylamine and 5-amino-1-pentanol in H_2SO_4 matrices (especially at high H_2SO_4

concentrations). Matrices such as sulfuric acid could also induce liquid-phase fragmentation of the organic species. Although the formation of salt crystals in solution is thought to negatively perturb the mass spectrometric response of the analytes⁷⁰, no suppression effects were observed in cation mode despite the strong ion pairs formed between sulfuric acid and basic organic species, and all organics could be identified even in 1M H₂SO₄ matrices. High concentrations of strong acids in the matrix therefore do not restrict the detection of organics in cation mode with impact ionization mass spectrometers at the concentrations investigated.

General rules for the mass spectral appearance of organic species in Europa-like ice grains. In Napoleoni et al.², we established generic rules for the detection of organics in NaCl-rich matrices using LILBID, and by extension, impact ionization mass spectrometry. We here summarize the list of rules established with salts (NaCl, MgSO₄) and H₂SO₄ matrices, to provide a complete set for the detection of organics in ice grains of typical Europa composition with SUDA:

- **sulfuric acid**

- sulfuric acid does not inhibit the detection of organics in cation mode even at high sulfuric acid concentrations. Indeed, all organic species in H₂SO₄ matrices show highly prominent protonated [M+H]⁺ peaks at all H₂SO₄ concentrations (0.01M-1M). The cation mass spectra of all organics in H₂SO₄ matrices are quite similar to the spectra of those organics in pure water matrices, with additional signatures due to the addition of H₂SO₄ molecules onto organic cations with increasing H₂SO₄ concentration.
- organic species in H₂SO₄ matrices typically form bisulfate adducts [M(HSO₄)]⁻ and/or [M(HSO₄)(H₂SO₄)_n]⁻ species, whereas deprotonated molecular peaks [M-H]⁻ are only observed for a few species in low H₂SO₄ concentrations. Bisulfate adducts can also form in MgSO₄ matrices for some organic species.

Generally, low pH matrices (i.e., having a high concentration of H^+) are expected to inhibit the formation of deprotonated molecular peaks $[M-H]^-$.

- **NaCl and MgSO₄ salts**

- in salt-rich matrices, protonated and deprotonated molecular peaks are usually suppressed with increasing salt concentrations, but organic species can still be detected via the presence of molecular ions and adducts with salt ions.
- in salt-rich samples, organic species form adducts with Na^+ and Mg^{2+} ions, but adduct formation with these two ions occurs via different mechanisms and results in different ions with different mass spectral properties. Sodiation seems more efficient than Magnesium-adduct formation and can lead to the formation of polysodiated adducts for organic species that contain hydroxyl and/or amine functional groups (i.e., carboxylic or amidic protons are replaced by Na^+). The formation of Mg-adducts accompanies the loss of a proton or addition of a negatively charged group (e.g., OH^-), thus forming singly charged ionic species. A wide variety of Mg-adducts can be formed.

- **Fragments.** We expect to detect a range of organic fragments in future SUDA mass spectra of European organic-rich ice grains, providing valuable structural information for the identification of parent organic species. Extensive fragmentation can be expected in sulfuric acid-rich ice grains (in cation mode), whereas the fragmentation will be limited with increasing matrix concentration in salt-rich ice grains and in sulfuric acid-rich ice grains in anion mode. The extent of the organic fragmentation will also be determined by the organic's structure and the presence of functional groups likely to be cleaved (e.g., hydroxyl, amine groups), and other parameters e.g., the impact velocity of the ice grain, the crystallinity of the water ice, and the spatial distribution of the organics and ions inside the water ice^{71,72}.

The mass spectrometric signal of most organics is generally higher in cation mode than in anion mode. However, the response greatly depends on the organics' chemical family and physicochemical properties. The pH is an important parameter that influences the formation and detectability of organic molecular ions, adducts and fragments, together with other physicochemical factors such as the organics' molecular structure or the presence of functional groups. We established characteristic mass spectral signatures of different organic families:

- **carboxylic acids**

- form highly prominent deprotonated molecular peaks $[M-H]^-$ in salt-rich matrices even at high salt concentration. Such peaks are also detected in H_2SO_4 matrices but with a lower intensity. Among the investigated compounds, this chemical family is the one to which anion polarity LILBID-MS is most sensitive in salt-rich matrices, although it is only moderately sensitive in H_2SO_4 solutions. Generally, we expect highly acidic compounds to be highly responsive in anion mode analysis thanks to a strong tendency to form deprotonated molecular peaks.
- typically form highly prominent $[M-OH]^+$ fragment peaks, as observed here in $MgSO_4$ and H_2SO_4 matrices and by Khawaja et al.⁸² in similar experiments with pure water matrix. This differs from the case of NaCl matrices where $[M-OH]^+$ peaks have a low intensity, but highly prominent disodiated $[M-H+2Na]^+$ peaks are observed².
- typically form a range of highly prominent Mg-adduct cations (e.g., $[M-H+Mg]^+$, $[M+Mg+OH]^+$...) in $MgSO_4$ matrices.

- **N-bearing organics**

- produce abundant characteristic peaks in cation mode in MgSO₄ and H₂SO₄ matrices, with highly prominent [M+H]⁺ peaks, and have a moderate response in NaCl matrices.
- these compounds have a much better response in cation mode than in anion mode in all investigated matrices (pure H₂O, NaCl, MgSO₄, H₂SO₄).
- **high pH organics** typically form highly prominent [2M+H+H₂SO₄]⁺ peaks in H₂SO₄ matrices.
- **aromatic rings** in organic species typically undergo a low degree of fragmentation, as seen for example with benzoic acid fragmenting to form highly prominent peaks of protonated benzene in H₂SO₄ matrices and of deprotonated benzene in MgSO₄ matrices.

Implications for Europa Clipper. SUDA's measurements will allow a compositional mapping of the surface by trajectory reconstruction of the ejecta particles^{29,30} providing accurate locations of measured/interpreted compositions. Together with the potential identification of organics, the analogue spectra presented here and in Napoleoni et al.² will help to determine the concentrations of NaCl, MgSO₄ and H₂SO₄ on the surface, by comparing the presence and relative abundances of ions in SUDA's mass spectra.

As Europa's trailing hemisphere is likely dominated by sulfuric acid hydrate (a product of surface radiolytic chemistry^{e.g.,39,56,58}), SUDA's measurements in cation mode in this hemisphere, with potentially lower salt concentrations, should undergo no suppression effects and therefore the assessment of organics on Europa's surface should be of high sensitivity and quality.

European ice grains are likely to have a more complex composition than the compositions investigated here, i.e., they may contain a variety of salts and organics instead of a binary

mixture of species. In matrices composed of complex mixtures, information can be deduced from mass spectral characteristics such as isotope patterns to help reduce ambiguities due to interferences. For example, for an organic species of molecular mass M , the $[M-H+Mg]^+$ and $[M+Na]^+$ cations have the same mass ($M+23u$). In the case of $[M-H+Mg]^+$, these two species can be differentiated from each other by Mg-isotope peaks at $M+24u$ and $M+25u$ at characteristic intensities. The identification of characteristic fragments could also help to constrain ambiguous identifications of organic species, as shown in this work by the identification of fragmentation patterns for typical functional groups.

The LILBID setup simulates different impact speeds of ice grains onto impact ionization mass spectrometers' detectors by adjustment of the laser power density and ion extraction parameters⁶⁴. The analogue mass spectra presented here were recorded with laser intensities of 95% to 100% and delay times of the gating system of 5.0 μs to 9.3 μs , which is representative of a speed regime of around 4-10 km/s. This speed regime includes the sampling speeds previously recommended^{65,71} for a maximum sensitivity to organic species and biosignatures (4–6 km/s). The speed of SUDA flybys is planned to be between 4 and 5 km/s³⁰.

The limits of detection (LODs) of organics in pure water matrix (Table 6) established in this work and the inferred suppression effects are a good approximation for SUDA or similar space detectors. In fact, detection limits of these space instruments are expected to be improved by at least one magnitude compared to our laboratory setup by the use of more efficient ion detectors (SUDA has a much higher dynamic range and therefore a higher sensitivity than the LILBID-ToF used here).

The results of our laboratory analogue experiments are applicable to other ocean worlds visited by Europa Clipper. For example, the icy surface of Ganymede is thought to contain large proportions of sulfuric acid and salts, likely sulfates⁸³. Sulfates might be recurring components

of icy ocean worlds, as they can be dominant products formed through the differentiation and evolution of subsurface oceans⁸⁴. Sulfuric acid hydrates are thought to be generally abundant material on the surface of the Galilean moons due to their formation mechanisms⁸⁵. The analogue mass spectra recorded with the LILBID experiment are stored in a database (<https://lilbid-db.planet.fu-berlin.de>)⁶⁷ that supports both Europa Clipper and the development of future ocean world missions, such as the proposed mission concept Enceladus Life Finder (ELF)⁸⁶, with the Enceladus Ice Analyzer (ENIA)⁸⁷ onboard.

Relevance for biosignature detection. Our analogue experiments established rules for the detection of organic material in European ice grains and include organic species that are relevant to astrobiology – e.g., sugars and N-heterocycles which play essential roles in all known biological processes^{88,89,90}. The range of investigated organic species cover relevant functional groups for astrobiological investigations of icy moons, since oxygen- and nitrogen-bearing as well as aromatics compounds have been detected in Enceladean ice grains^{25,26}. The experiments covered general classes of organic compounds in a generic approach, so that results are potentially applicable to a variety of diverse agnostic biosignatures. Previous LILBID experiments targeting terrestrial biosignatures were conducted with bacterial extracts, amino acids, fatty acids and peptides and showed that these materials are detectable by SUDA-type mass spectrometers even at low concentrations^{1,65,66}. The rules established here could help the detection of more, and potentially yet unknown, organic biosignatures of alien lifeforms.

5 Conclusions & Outlook

Europa's ocean and ice crust are expected to contain high proportions of non-water constituents such as sulfates and sulfuric acid^{33-36,39,56,58}. In this work, we simulated the mass spectra of organic-rich ice grains mixed with these compounds as expected to be produced by SUDA-type impact ionization mass spectrometers. We performed analogue experiments with the

LILBID technique and measured seven organic species, representative of a wide range of chemical families, in magnesium sulfate and sulfuric acid liquid matrices at 0.01M, 0.1M and 1M concentrations.

Our results showed that SUDA will be more sensitive to the majority of the measured organics and their fragments in cation mode than in anion mode. The higher sensitivity in cation mode is particularly enhanced for sulfuric acid matrices (i.e., no suppression effects were observed in cation mode and the organic signal was as high as in pure water). The reason is that the only cation species sulfuric acid releases in water is H^+ , whereas salt matrices release cations such as alkali metals (e.g., Na^+) which induce suppression effects. A better sensitivity in cation mode than anion mode was also previously found for organics in NaCl matrices².

The cation mode enhanced sensitivity to organics in sulfuric acid matrices may serendipitously serve the Europa Clipper observations well. Endogenous organics should be associated with oceanic salts, such as NaCl and $MgSO_4$, and thus we predict that if organics are to be found on Europa, they would likely be associated with those salts. Conversely, sulfuric acid is an exogenous radiolytic product and there is no a priori reason to expect a direct association with endogenous organics. In addition, the radiolytic processing that generates sulfuric acid may also modify any organics that are present⁹¹. As a result, it is reasonable to predict that lower concentrations of organics might be associated with sulfuric acid-rich regions, relative to salt-rich regions. Thus, SUDA's enhanced organic sensitivity in cation mode to organics associated with sulfuric acid is advantageous, given the above considerations for the European environment.

Importantly, we emphasize the necessity of both ion modes in spaceborne impact ionization mass spectrometers to cover a wide range of organic families (e.g., anion mode is more sensitive to non-polar compounds such lipids). Both SUDA¹⁷ and the Enceladus Ice Analyzer

instrument (ENIA)⁸⁷, in a proposed astrobiology mission concept to Enceladus (Enceladus Life Finder)⁸⁶, will be capable of detecting cations and anions.

Our experiments show that the detection of organic species in ice grains by SUDA can be possible despite the potentially complex inorganic ice matrices. Suppression effects reduce the sensitivity to the organics in the presence of Na-chlorides² and Mg-sulfates, but not in the presence of sulfuric acid. We established generic rules applicable to a wide range of organic species, which may allow the discovery of organic biosignatures in European ice grains. This study provides valuable experimental context for the interpretation of impact ionization mass spectra of SUDA-type instruments at relevant impact speeds, and for space mission planning (e.g., use of cation or anion modes, compositional locations to target). This work will also significantly enhance our ability to interpret the origin and evolution of organic material on Europa, possibly providing insights into hydrothermal sources in the subsurface ocean, interactions with salts and inorganic material, transport from the subsurface ocean to the surface and lastly modification via surface processes such as irradiation by magnetospheric particles. These processes may all be part of the pathway of organic material toward finally be detected in a dust cloud of ice particles by the Europa Clipper mission.

ASSOCIATED CONTENT

Supporting Information. Figures S1 – S36; Tables S1 & S2.

The figures S1 – S36 are supplementary mass spectra mentioned in the main manuscript. Tables S1 and S2 gather identifications of fragment ions in cation and anion modes, respectively, for the different samples.

AUTHOR INFORMATION

*corresponding author: m.napoleoni@fu-berlin.de

ACKNOWLEDGMENT

This work was conducted at Freie Universität Berlin and supported by the European Research Council (ERC) under the European Union's Horizon 2020 research and innovation program by the Consolidator Grant 724908 Habitat-OASIS.

ABBREVIATIONS

CDA, Cosmic Dust Analyzer; ENIA, Enceladus Ice Analyzer; ELF, Enceladus Life Finder mission; ESI, electrospray ionization; LILBID, Laser Induced Liquid Beam Ion Desorption; LOD, Limits Of Detection; MALDI, Matrix Assisted Laser Desorption Ionization; MS, mass spectrometry; NIST, National Institute of Standards and Technology; SUDA, SURface Dust Analyzer; TOF, time-of-flight.

REFERENCES

- (1) Klenner, F.; Postberg, F.; Hillier, J.; Khawaja, N.; Cable, M. L.; Abel, B.; Kempf, S.; Glein, C. R.; Lunine, J. I.; Hodyss, R.; Reviol, R.; Stolz, F. Discriminating Abiotic and Biotic Fingerprints of Amino Acids and Fatty Acids in Ice Grains Relevant to Ocean Worlds. *Astrobiology* **2020**, *20* (10), 1168–1184. <https://doi.org/10.1089/ast.2019.2188>.
- (2) Napoleoni, M.; Klenner, F.; Khawaja, N.; Hillier, J. K.; Postberg, F. Mass Spectrometric Fingerprints of Organic Compounds in NaCl-Rich Ice Grains from Europa and Enceladus. *ACS Earth Space Chem.* **2023**, acsearthspacechem.2c00342. <https://doi.org/10.1021/acsearthspacechem.2c00342>.
- (3) Carr, M. H.; Belton, M. J. S.; Chapman, C. R.; Davies, M. E.; Geissler, P.; Greenberg, R.; McEwen, A. S.; Tufts, B. R.; Greeley, R.; Sullivan, R.; Head, J. W.; Pappalardo, R. T.; Klaasen, K. P.; Johnson, T. V.; Kaufman, J.; Senske, D.; Moore, J.; Neukum, G.; Schubert, G.; Burns, J. A.; Thomas, P.; Veverka, J. Evidence for a Subsurface Ocean on Europa. *Nature* **1998**, *391* (6665), 363–365. <https://doi.org/10.1038/34857>.
- (4) Kivelson, M. G.; Khurana, K. K.; Russell, C. T.; Volwerk, M.; Walker, R. J.; Zimmer, C. Galileo Magnetometer Measurements: A Stronger Case for a Subsurface Ocean at Europa. *Science* **2000**, *289* (5483), 1340–1343. <https://doi.org/10.1126/science.289.5483.1340>.
- (5) Collins, G. C.; Goodman, J. C. Enceladus' South Polar Sea. *Icarus* **2007**, *189* (1), 72–82. <https://doi.org/10.1016/j.icarus.2007.01.010>.

- (6) Spohn, T.; Schubert, G. Oceans in the Icy Galilean Satellites of Jupiter? *Icarus* **2003**, *161* (2), 456–467. [https://doi.org/10.1016/S0019-1035\(02\)00048-9](https://doi.org/10.1016/S0019-1035(02)00048-9).
- (7) Khurana, K. K.; Kivelson, M. G.; Stevenson, D. J.; Schubert, G.; Russell, C. T.; Walker, R. J.; Polanskey, C. Induced Magnetic Fields as Evidence for Subsurface Oceans in Europa and Callisto. *Nature* **1998**, *395* (6704), 777–780. <https://doi.org/10.1038/27394>.
- (8) Hendrix, A. R.; Hurford, T. A.; Barge, L. M.; Bland, M. T.; Bowman, J. S.; Brinckerhoff, W.; Buratti, B. J.; Cable, M. L.; Castillo-Rogez, J.; Collins, G. C.; Diniega, S.; German, C. R.; Hayes, A. G.; Hoehler, T.; Hosseini, S.; Howett, C. J. A.; McEwen, A. S.; Neish, C. D.; Neveu, M.; Nordheim, T. A.; Patterson, G. W.; Patthoff, D. A.; Phillips, C.; Rhoden, A.; Schmidt, B. E.; Singer, K. N.; Soderblom, J. M.; Vance, S. D. The NASA Roadmap to Ocean Worlds. *Astrobiology* **2019**, *19* (1), 1–27. <https://doi.org/10.1089/ast.2018.1955>.
- (9) Lunine, J. I. Ocean Worlds Exploration. *Acta Astronautica* **2017**, *131*, 123–130. <https://doi.org/10.1016/j.actaastro.2016.11.017>.
- (10) Roth, L.; Saur, J.; Retherford, K. D.; Strobel, D. F.; Feldman, P. D.; McGrath, M. A.; Nimmo, F. Transient Water Vapor at Europa's South Pole. *Science* **2014**, *343* (6167), 171–174. <https://doi.org/10.1126/science.1247051>.
- (11) Dougherty, M. K.; Khurana, K. K.; Neubauer, F. M.; Russell, C. T.; Saur, J.; Leisner, J. S.; Burton, M. E. Identification of a Dynamic Atmosphere at Enceladus with the Cassini Magnetometer. *Science* **2006**, *311* (5766), 1406–1409. <https://doi.org/10.1126/science.1120985>.
- (12) Hansen, C. J.; Esposito, L.; Stewart, A. I. F.; Colwell, J.; Hendrix, A.; Pryor, W.; Shemansky, D.; West, R. Enceladus' Water Vapor Plume. *Science* **2006**, *311* (5766), 1422–1425. <https://doi.org/10.1126/science.1121254>.
- (13) Porco, C. C.; Helfenstein, P.; Thomas, P. C.; Ingersoll, A. P.; Wisdom, J.; West, R.; Neukum, G.; Denk, T.; Wagner, R.; Roatsch, T.; Kieffer, S.; Turtle, E.; McEwen, A.; Johnson, T. V.; Rathbun, J.; Veverka, J.; Wilson, D.; Perry, J.; Spitale, J.; Brahic, A.; Burns, J. A.; DelGenio, A. D.; Dones, L.; Murray, C. D.; Squyres, S. Cassini Observes the Active South Pole of Enceladus. *Science* **2006**, *311* (5766), 1393–1401. <https://doi.org/10.1126/science.1123013>.
- (14) Spahn, F.; Schmidt, J.; Albers, N.; Hörning, M.; Makuch, M.; Seiß, M.; Kempf, S.; Srama, R.; Dikarev, V.; Helfert, S.; Moragas-Klostermeyer, G.; Krivov, A. V.; Sremčević, M.; Tuzzolino, A. J.; Economou, T.; Grün, E. Cassini Dust Measurements at Enceladus and Implications for the Origin of the E Ring. *Science* **2006**, *311* (5766), 1416–1418. <https://doi.org/10.1126/science.1121375>.
- (15) V. Krivov, A.; Sremčević, M.; Spahn, F.; Dikarev, V. V.; Kholoshevnikov, K. V. Impact-Generated Dust Clouds around Planetary Satellites: Spherically Symmetric Case. *Planetary and Space Science* **2003**, *51* (3), 251–269. [https://doi.org/10.1016/S0032-0633\(02\)00147-2](https://doi.org/10.1016/S0032-0633(02)00147-2).
- (16) Miljković, K.; Hillier, J. K.; Mason, N. J.; Zarnecki, J. C. Models of Dust around Europa and Ganymede. *Planetary and Space Science* **2012**, *70* (1), 20–27. <https://doi.org/10.1016/j.pss.2012.06.006>.

- (17) Kempf S., Altobelli N., Briois C., et al. (2014) SUDA: a dust mass spectrometer for compositional surface mapping for a mission to Europa. *Eur Planet Sci Congr* 2014:229.
- (18) Howell, S. M.; Pappalardo, R. T. NASA's Europa Clipper—a Mission to a Potentially Habitable Ocean World. *Nat Commun* **2020**, *11* (1), 1311. <https://doi.org/10.1038/s41467-020-15160-9>.
- (19) Srama, R.; Ahrens, T. J.; Altobelli, N.; Auer, S.; Bradley, J. G.; Burton, M.; Dikarev, V. V.; Economou, T.; Fechtig, H.; Görlich, M.; Grande, M.; Graps, A.; Grün, E.; Havnes, O.; Helfert, S.; Horanyi, M.; Igenbergs, E.; Jessberger, E. K.; Johnson, T. V.; Kempf, S.; Krivov, A. V.; Krüger, H.; Mocker-Ahlreep, A.; Moragas-Klostermeyer, G.; Lamy, P.; Landgraf, M.; Linkert, D.; Linkert, G.; Lura, F.; McDonnell, J. A. M.; Möhlmann, D.; Morfill, G. E.; Müller, M.; Roy, M.; Schäfer, G.; Schlotzhauer, G.; Schwehm, G. H.; Spahn, F.; Stübig, M.; Svestka, J.; Tschernjawski, V.; Tuzzolino, A. J.; Wäsch, R.; Zook, H. A. The Cassini Cosmic Dust Analyzer. *Space Sci Rev* **2004**, *114* (1–4), 465–518. <https://doi.org/10.1007/s11214-004-1435-z>.
- (20) Hillier, J.; Green, S.; Mcbride, N.; Altobelli, N.; Postberg, F.; Kempf, S.; Schwanethal, J.; Srama, R.; McDonnell, J.; Grun, E. Interplanetary Dust Detected by the Cassini CDA Chemical Analyser. *Icarus* **2007**, *190* (2), 643–654. <https://doi.org/10.1016/j.icarus.2007.03.024>.
- (21) Postberg, F.; Kempf, S.; Schmidt, J.; Brilliantov, N.; Beinsen, A.; Abel, B.; Buck, U.; Srama, R. Sodium Salts in E-Ring Ice Grains from an Ocean below the Surface of Enceladus. *Nature* **2009**, *459* (7250), 1098–1101. <https://doi.org/10.1038/nature08046>.
- (22) Postberg, F.; Schmidt, J.; Hillier, J.; Kempf, S.; Srama, R. A Salt-Water Reservoir as the Source of a Compositionally Stratified Plume on Enceladus. *Nature* **2011**, *474* (7353), 620–622. <https://doi.org/10.1038/nature10175>.
- (23) Postberg, F., Sekine, Y., Klenner, F. et al. Detection of phosphates originating from Enceladus's ocean. *Nature* **2023**, *618*, 489–493. <https://doi.org/10.1038/s41586-023-05987-9>
- (24) Postberg, F.; Kempf, S.; Hillier, J. K.; Srama, R.; Green, S. F.; McBride, N.; Grün, E. The E-Ring in the Vicinity of Enceladus. *Icarus* **2008**, *193* (2), 438–454. <https://doi.org/10.1016/j.icarus.2007.09.001>.
- (25) Postberg, F.; Khawaja, N.; Abel, B.; Choblet, G.; Glein, C. R.; Gudipati, M. S.; Henderson, B. L.; Hsu, H.-W.; Kempf, S.; Klenner, F.; Moragas-Klostermeyer, G.; Magee, B.; Nölle, L.; Perry, M.; Reviol, R.; Schmidt, J.; Srama, R.; Stolz, F.; Tobie, G.; Trieloff, M.; Waite, J. H. Macromolecular Organic Compounds from the Depths of Enceladus. *Nature* **2018**, *558* (7711), 564–568. <https://doi.org/10.1038/s41586-018-0246-4>.
- (26) Khawaja, N.; Postberg, F.; Hillier, J.; Klenner, F.; Kempf, S.; Nölle, L.; Reviol, R.; Zou, Z.; Srama, R. Low-Mass Nitrogen-, Oxygen-Bearing, and Aromatic Compounds in Enceladean Ice Grains. *Monthly Notices of the Royal Astronomical Society* **2019**, *489* (4), 5231–5243. <https://doi.org/10.1093/mnras/stz2280>.
- (27) Postberg, F.; Grün, E.; Horanyi, M.; Kempf, S.; Krüger, H.; Schmidt, J.; Spahn, F.; Srama, R.; Sternovsky, Z.; Trieloff, M. Compositional Mapping of Planetary Moons by Mass Spectrometry of Dust Ejecta. *Planetary and Space Science* **2011**, *59* (14), 1815–1825. <https://doi.org/10.1016/j.pss.2011.05.001>.

- (28) Kempf, S.; Srama, R.; Grün, E.; Mocker, A.; Postberg, F.; Hillier, J. K.; Horányi, M.; Sternovsky, Z.; Abel, B.; Beinsen, A.; Thissen, R.; Schmidt, J.; Spahn, F.; Altobelli, N. Linear High Resolution Dust Mass Spectrometer for a Mission to the Galilean Satellites. *Planetary and Space Science* **2012**, *65* (1), 10–20. <https://doi.org/10.1016/j.pss.2011.12.019>.
- (29) Goode, W.; Kempf, S.; Schmidt, J. Detecting the Surface Composition of Geological Features on Europa and Ganymede Using a Surface Dust Analyzer. *Planetary and Space Science* **2021**, *208*, 105343. <https://doi.org/10.1016/j.pss.2021.105343>.
- (30) Goode, W.; Kempf, S.; Schmidt, J. Mapping the Surface Composition of Europa with SUDA. *Planetary and Space Science* **2023**, *227*, 105633. <https://doi.org/10.1016/j.pss.2023.105633>.
- (31) Hand, K. P.; Carlson, R. W. Europa's Surface Color Suggests an Ocean Rich with Sodium Chloride: Sodium Chloride on Europa's Surface. *Geophys. Res. Lett.* **2015**, *42* (9), 3174–3178. <https://doi.org/10.1002/2015GL063559>.
- (32) Trumbo, S. K.; Brown, M. E.; Hand, K. P. Sodium Chloride on the Surface of Europa. *Sci. Adv.* **2019**, *5* (6), eaaw7123. <https://doi.org/10.1126/sciadv.aaw7123>.
- (33) McCord, T. B.; Hansen, G. B.; Fanale, F. P.; Carlson, R. W.; Matson, D. L.; Johnson, T. V.; Smythe, W. D.; Crowley, J. K.; Martin, P. D.; Ocampo, A.; Hibbitts, C. A.; Granahan, J. C.; the NIMS Team. Salts on Europa's Surface Detected by Galileo's Near Infrared Mapping Spectrometer. *Science* **1998**, *280* (5367), 1242–1245. <https://doi.org/10.1126/science.280.5367.1242>.
- (34) Dalton, J. B. Linear Mixture Modeling of Europa's Non-Ice Material Based on Cryogenic Laboratory Spectroscopy. *Geophys. Res. Lett.* **2007**, *34* (21), L21205. <https://doi.org/10.1029/2007GL031497>.
- (35) Hibbitts, C. A.; Stockstill-Cahill, K.; Wing, B.; Paranicas, C. Color Centers in Salts - Evidence for the Presence of Sulfates on Europa. *Icarus* **2019**, *326*, 37–47. <https://doi.org/10.1016/j.icarus.2019.02.022>.
- (36) Cruz Mermy, G.; Schmidt, F.; Andrieu, F.; Cornet, T.; Belgacem, I.; Altobelli, N. Selection of Chemical Species for Europa's Surface Using Galileo/NIMS. *Icarus* **2023**, *394*, 115379. <https://doi.org/10.1016/j.icarus.2022.115379>.
- (37) Carlson, R. W., Calvin, W. M., Dalton, J. B., Hansen, G. B., Hudson, R. L., Johnson, R. E., ... & Moore, M. H. (2009). Europa's surface composition. *Europa*, 283.
- (38) Zolotov, M. Y.; Shock, E. L. Composition and Stability of Salts on the Surface of Europa and Their Oceanic Origin. *J. Geophys. Res.* **2001**, *106* (E12), 32815–32827. <https://doi.org/10.1029/2000JE001413>.
- (39) Brown, M. E.; Hand, K. P. SALTS AND RADIATION PRODUCTS ON THE SURFACE OF EUROPA. *AJ* **2013**, *145* (4), 110. <https://doi.org/10.1088/0004-6256/145/4/110>.
- (40) King, O.; Fletcher, L. N.; Ligier, N. Compositional Mapping of Europa Using MCMC Modeling of Near-IR VLT/SPHERE and Galileo/NIMS Observations. *Planet. Sci. J.* **2022**, *3* (3), 72. <https://doi.org/10.3847/PSJ/ac596d>.

- (41) Eviatar, A.; Siscoe, G. L.; Johnson, T. V.; Matson, D. L. Effects of Io Ejecta on Europa. *Icarus* **1981**, *47* (1), 75–83. [https://doi.org/10.1016/0019-1035\(81\)90092-0](https://doi.org/10.1016/0019-1035(81)90092-0).
- (42) Bagenal, F.; Dols, V. The Space Environment of Io and Europa. *JGR Space Physics* **2020**, *125* (5). <https://doi.org/10.1029/2019JA027485>.
- (43) McCord, T. B. Brines Exposed to Europa Surface Conditions. *J. Geophys. Res.* **2002**, *107* (E1), 5004. <https://doi.org/10.1029/2000JE001453>.
- (44) Fanale, F. P.; Li, Y.-H.; De Carlo, E.; Farley, C.; Sharma, S. K.; Horton, K.; Granahan, J. C. An Experimental Estimate of Europa's "Ocean" Composition Independent of Galileo Orbital Remote Sensing. *J. Geophys. Res.* **2001**, *106* (E7), 14595–14600. <https://doi.org/10.1029/2000JE001385>.
- (45) Cooper, J. Energetic Ion and Electron Irradiation of the Icy Galilean Satellites. *Icarus* **2001**, *149* (1), 133–159. <https://doi.org/10.1006/icar.2000.6498>.
- (46) Nordheim, T. A.; Jasinski, J. M.; Hand, K. P. Galactic Cosmic-Ray Bombardment of Europa's Surface. *ApJ* **2019**, *881* (2), L29. <https://doi.org/10.3847/2041-8213/ab3661>.
- (47) Moore, M. IR Detection of H₂O₂ at 80 K in Ion-Irradiated Laboratory Ices Relevant to Europa. *Icarus* **2000**, *145* (1), 282–288. <https://doi.org/10.1006/icar.1999.6325>.
- (48) Orlando, T. M.; Sieger, M. T. The Role of Electron-Stimulated Production of O₂ from Water Ice in the Radiation Processing of Outer Solar System Surfaces. *Surface Science* **2003**, *528* (1–3), 1–7. [https://doi.org/10.1016/S0039-6028\(02\)02602-X](https://doi.org/10.1016/S0039-6028(02)02602-X).
- (49) Loeffler, M.; Raut, U.; Vidal, R.; Baragiola, R.; Carlson, R. Synthesis of Hydrogen Peroxide in Water Ice by Ion Irradiation. *Icarus* **2006**, *180* (1), 265–273. <https://doi.org/10.1016/j.icarus.2005.08.001>.
- (50) Zheng, W.; Jewitt, D.; Kaiser, R. I. Formation of Hydrogen, Oxygen, and Hydrogen Peroxide in Electron-irradiated Crystalline Water Ice. *ApJ* **2006**, *639* (1), 534–548. <https://doi.org/10.1086/499231>.
- (51) Teolis, B. D.; Loeffler, M. J.; Raut, U.; Famá, M.; Baragiola, R. A. Ozone Synthesis on the Icy Satellites. *ApJ* **2006**, *644* (2), L141–L144. <https://doi.org/10.1086/505743>.
- (52) Hand, K. P.; Carlson, R. W. H₂O₂ Production by High-Energy Electrons on Icy Satellites as a Function of Surface Temperature and Electron Flux. *Icarus* **2011**, *215* (1), 226–233. <https://doi.org/10.1016/j.icarus.2011.06.031>.
- (53) Carlson, R. W.; Anderson, M. S.; Johnson, R. E.; Smythe, W. D.; Hendrix, A. R.; Barth, C. A.; Soderblom, L. A.; Hansen, G. B.; McCord, T. B.; Dalton, J. B.; Clark, R. N.; Shirley, J. H.; Ocampo, A. C.; Matson, D. L. Hydrogen Peroxide on the Surface of Europa. *Science* **1999**, *283* (5410), 2062–2064. <https://doi.org/10.1126/science.283.5410.2062>.
- (54) Tribbett, P. D.; Loeffler, M. J. Thermal Reactions between H₂S and O₃: Implications for Europa Surface Chemistry. *Planet. Sci. J.* **2022**, *3* (10), 233. <https://doi.org/10.3847/PSJ/ac9236>.

- (55) Carlson, R. W.; Anderson, M. S.; Johnson, R. E.; Schulman, M. B.; Yavrouian, A. H. Sulfuric Acid Production on Europa: The Radiolysis of Sulfur in Water Ice. *Icarus* **2002**, *157* (2), 456–463. <https://doi.org/10.1006/icar.2002.6858>.
- (56) Carlson, R. W.; Anderson, M. S.; Mehlman, R.; Johnson, R. E. Distribution of Hydrate on Europa: Further Evidence for Sulfuric Acid Hydrate. *Icarus* **2005**, *177* (2), 461–471. <https://doi.org/10.1016/j.icarus.2005.03.026>.
- (57) Strazzulla, G.; Baratta, G. A.; Leto, G.; Gomis, O. Hydrate Sulfuric Acid after Sulfur Implantation in Water Ice. *Icarus* **2007**, *192* (2), 623–628. <https://doi.org/10.1016/j.icarus.2007.08.004>.
- (58) Ligier, N.; Poulet, F.; Carter, J.; Brunetto, R.; Gourgeot, F. VLT/SINFONI OBSERVATIONS OF EUROPA: NEW INSIGHTS INTO THE SURFACE COMPOSITION. *The Astronomical Journal* **2016**, *151* (6), 163. <https://doi.org/10.3847/0004-6256/151/6/163>.
- (59) Mishra, I.; Lewis, N.; Lunine, J.; Hand, K. P.; Helfenstein, P.; Carlson, R. W.; MacDonald, R. J. A Comprehensive Revisit of Select Galileo/NIMS Observations of Europa. *Planet. Sci. J.* **2021**, *2* (5), 183. <https://doi.org/10.3847/PSJ/ac1acb>.
- (60) Fischer, P. D.; Brown, M. E.; Hand, K. P. SPATIALLY RESOLVED SPECTROSCOPY OF EUROPA: THE DISTINCT SPECTRUM OF LARGE-SCALE CHAOS. *AJ* **2015**, *150* (5), 164. <https://doi.org/10.1088/0004-6256/150/5/164>.
- (61) Shirley, J. H.; Dalton, J. B.; Prockter, L. M.; Kamp, L. W. Europa's Ridged Plains and Smooth Low Albedo Plains: Distinctive Compositions and Compositional Gradients at the Leading Side–Trailing Side Boundary. *Icarus* **2010**, *210* (1), 358–384. <https://doi.org/10.1016/j.icarus.2010.06.018>.
- (62) Kleinekofort, W.; Avdiev, J.; Brutschy, B. A New Method of Laser Desorption Mass Spectrometry for the Study of Biological Macromolecules. *International Journal of Mass Spectrometry and Ion Processes* **1996**, *152* (2–3), 135–142. [https://doi.org/10.1016/0168-1176\(95\)04330-6](https://doi.org/10.1016/0168-1176(95)04330-6).
- (63) Kleinekofort, W.; Pfenninger, A.; Plomer, T.; Griesinger, C.; Brutschy, B. Observation of Noncovalent Complexes Using Laser-Induced Liquid Beam Ionization/Desorption. *International Journal of Mass Spectrometry and Ion Processes* **1996**, *156* (3), 195–202. [https://doi.org/10.1016/S0168-1176\(96\)04507-7](https://doi.org/10.1016/S0168-1176(96)04507-7).
- (64) Klenner, F.; Postberg, F.; Hillier, J.; Khawaja, N.; Reviol, R.; Srama, R.; Abel, B.; Stolz, F.; Kempf, S. Analogue Spectra for Impact Ionization Mass Spectra of Water Ice Grains Obtained at Different Impact Speeds in Space. *Rapid Commun Mass Spectrom* **2019**, *33* (22), 1751–1760. <https://doi.org/10.1002/rcm.8518>.
- (65) Klenner, F.; Postberg, F.; Hillier, J.; Khawaja, N.; Reviol, R.; Stolz, F.; Cable, M. L.; Abel, B.; Nölle, L. Analog Experiments for the Identification of Trace Biosignatures in Ice Grains from Extraterrestrial Ocean Worlds. *Astrobiology* **2020**, *20* (2), 179–189. <https://doi.org/10.1089/ast.2019.2065>.
- (66) Dannenmann, M.; Klenner, F.; Bönigk, J.; Pavlista, M.; Napoleoni, M.; Hillier, J.; Khawaja, N.; Olsson-Francis, K.; Cable, M. L.; Malaska, M. J.; Abel, B.; Postberg, F. Toward Detecting Biosignatures of DNA, Lipids, and Metabolic Intermediates from Bacteria in Ice

Grains Emitted by Enceladus and Europa. *Astrobiology* **2023**, *23* (1), 60–75. <https://doi.org/10.1089/ast.2022.0063>.

(67) Klenner, F.; Umair, M.; Walter, S. H. G.; Khawaja, N.; Hillier, J.; Nölle, L.; Zou, Z.; Napoleoni, M.; Sanderink, A.; Zuschneid, W.; Abel, B.; Postberg, F. Developing a Laser Induced Liquid Beam Ion Desorption Spectral Database as Reference for Spaceborne Mass Spectrometers. *Earth and Space Science* **2022**, *9* (9). <https://doi.org/10.1029/2022EA002313>.

(68) Piwowar, A. M.; Lockyer, N. P.; Vickerman, J. C. Salt Effects on Ion Formation in Desorption Mass Spectrometry: An Investigation into the Role of Alkali Chlorides on Peak Suppression in Time-of-Flight-Secondary Ion Mass Spectrometry. *Anal. Chem.* **2009**, *81* (3), 1040–1048. <https://doi.org/10.1021/ac8020888>.

(69) Knochenmuss, R.; Dubois, F.; Dale, M. J.; Zenobi, R. The Matrix Suppression Effect and Ionization Mechanisms in Matrix-Assisted Laser Desorption/Ionization. *Rapid Commun. Mass Spectrom.* **1996**, *10* (8), 871–877. [https://doi.org/10.1002/\(SICI\)1097-0231\(19960610\)10:8<871::AID-RCM559>3.0.CO;2-R](https://doi.org/10.1002/(SICI)1097-0231(19960610)10:8<871::AID-RCM559>3.0.CO;2-R).

(70) King, R.; Bonfiglio, R.; Fernandez-Metzler, C.; Miller-Stein, C.; Olah, T. Mechanistic Investigation of Ionization Suppression in Electrospray Ionization. *J. Am. Soc. Mass Spectrom.* **2000**, *11* (11), 942–950. [https://doi.org/10.1016/S1044-0305\(00\)00163-X](https://doi.org/10.1016/S1044-0305(00)00163-X).

(71) Jaramillo-Botero, A.; Cable, M. L.; Hofmann, A. E.; Malaska, M.; Hodyss, R.; Lunine, J. Understanding Hypervelocity Sampling of Biosignatures in Space Missions. *Astrobiology* **2021**, *21* (4), 421–442. <https://doi.org/10.1089/ast.2020.2301>.

(72) Schulze, J. A.; Yilmaz, D. E.; Cable, M. L.; Malaska, M.; Hofmann, A. E.; Hodyss, R. P.; Lunine, J. I.; van Duin, A. C. T.; Jaramillo-Botero, A. Effect of Salts on the Formation and Hypervelocity-Induced Fragmentation of Icy Clusters with Embedded Amino Acids. *ACS Earth Space Chem.* **2022**, acsearthspacechem.2c00267. <https://doi.org/10.1021/acsearthspacechem.2c00267>.

(73) Khawaja, N.; Hillier, J.; Klenner, F.; Nölle, L.; Zou, Z.; Napoleoni, M.; Reviol, R.; Postberg, F. Complementary Mass Spectral Analysis of Isomeric O-Bearing Organic Compounds and Fragmentation Differences through Analog Techniques for Spaceborne Mass Spectrometers. *Planet. Sci. J.* **2022**, *3* (11), 254. <https://doi.org/10.3847/PSJ/ac97ed>.

(74) Shi, T.; Zhao, J.; Shek, P. I.; Hopkinson, A. C.; Siu, K. M. Carbonate, Carbamate, Urea, and Guanidine as Model Species for Functional Groups in Biological Molecules A Combined Density Functional Theory and Mass Spectrometry Examination of Polysodiation and Gas-Phase Dissociation. *Can. J. Chem.* **2005**, *83* (11), 1941–1952. <https://doi.org/10.1139/v05-204>.

(75) Han, L.; Costello, C. E. Electron Transfer Dissociation of Milk Oligosaccharides. *J. Am. Soc. Mass Spectrom.* **2011**, *22* (6), 997–1013. <https://doi.org/10.1007/s13361-011-0117-9>.

(76) Newton, K. A.; McLuckey, S. A. Generation and Manipulation of Sodium Cationized Peptides in the Gas Phase. *J. Am. Soc. Mass Spectrom.* **2004**, *15* (4), 607–615. <https://doi.org/10.1016/j.jasms.2003.12.014>.

(77) Wong, A. W.; Wang, H.; Lebrilla, C. B. Selection of Anionic Dopant for Quantifying Desialylation Reactions with MALDI-FTMS. *Anal. Chem.* **2000**, *72* (7), 1419–1425. <https://doi.org/10.1021/ac990956w>.

- (78) Jiang, Y.; Cole, R. B. Oligosaccharide Analysis Using Anion Attachment in Negative Mode Electrospray Mass Spectrometry. *J. Am. Soc. Mass Spectrom.* **2005**, *16* (1), 60–70. <https://doi.org/10.1016/j.jasms.2004.09.006>.
- (79) Boutegrabet, L.; Kanawati, B.; Gebefügi, I.; Peyron, D.; Cayot, P.; Gougeon, R. D.; Schmitt-Kopplin, P. Attachment of Chloride Anion to Sugars: Mechanistic Investigation and Discovery of a New Dopant for Efficient Sugar Ionization/Detection in Mass Spectrometers. *Chem. Eur. J.* **2012**, *18* (41), 13059–13067. <https://doi.org/10.1002/chem.201103788>.
- (80) Phungsai, P.; Kurisu, F.; Kasuga, I.; Furumai, H. Molecular Characterization of Low Molecular Weight Dissolved Organic Matter in Water Reclamation Processes Using Orbitrap Mass Spectrometry. *Water Research* **2016**, *100*, 526–536. <https://doi.org/10.1016/j.watres.2016.05.047>.
- (81) Chowdhury, S. K.; Katta, V.; Beavis, R. C.; Chait, B. T. Origin and Removal of Adducts (Molecular Mass = 98 u) Attached to Peptide and Protein Ions in Electrospray Ionization Mass Spectra. *J. Am. Soc. Mass Spectrom.* **1990**, *1* (5), 382–388. [https://doi.org/10.1016/1044-0305\(90\)85018-H](https://doi.org/10.1016/1044-0305(90)85018-H).
- (82) Khawaja, N.; O’Sullivan, T.; Klenner, F.; Sanchez, Lucia H.; and Hillier, J. Discriminating Aromatic Parent Compounds and their Derivative Isomers in Ice Grains from Enceladus and Europa using a Laboratory Analogue for Spaceborne Mass Spectrometers. **2023** In review, *ESS*
- (83) Ligier, N.; Paranicas, C.; Carter, J.; Poulet, F.; Calvin, W. M.; Nordheim, T. A.; Snodgrass, C.; Ferellec, L. Surface Composition and Properties of Ganymede: Updates from Ground-Based Observations with the near-Infrared Imaging Spectrometer SINFONI/VLT/ESO. *Icarus* **2019**, *333*, 496–515. <https://doi.org/10.1016/j.icarus.2019.06.013>.
- (84) Sohl, F.; Choukroun, M.; Kargel, J.; Kimura, J.; Pappalardo, R.; Vance, S.; Zolotov, M. Subsurface Water Oceans on Icy Satellites: Chemical Composition and Exchange Processes. *Space Sci Rev* **2010**, *153* (1–4), 485–510. <https://doi.org/10.1007/s11214-010-9646-y>.
- (85) Maynard-Casely, H. E.; Wallwork, K. S.; Avdeev, M. A New Material for the Icy Galilean Moons: The Structure of Sulfuric Acid Hexahydrate: A NEW MATERIAL FOR THE GALILEAN MOONS. *J. Geophys. Res. Planets* **2013**, *118* (9), 1895–1902. <https://doi.org/10.1002/jgre.20124>.
- (86) Reh, K.; Spilker, L., Lunine; J. I., Waite; J. H., Cable; M. L., Postberg; F., & Clark, K. (2016, March). Enceladus Life Finder: The search for life in a habitable moon. In 2016 IEEE Aerospace Conference (pp. 1-8). IEEE.
- (87) Srama, R., Postberg, F., Henkel, H., Klopfer, T., Li, Y., Simolka, J., ... & Spohn, T. (2015). Enceladus Icy Jet Analyzer (ENIJA): Search for life with a high resolution TOF-MS for in situ characterization of high dust density regions. *Eur. Planet. Sci. Congr.*, 10.
- (88) Stern, R.; Jędrzejak, M. J. Carbohydrate Polymers at the Center of Life’s Origins: The Importance of Molecular Processivity. *Chem. Rev.* **2008**, *108* (12), 5061–5085. <https://doi.org/10.1021/cr078240l>.
- (89) Furukawa, Y.; Chikaraishi, Y.; Ohkouchi, N.; Ogawa, N. O.; Glavin, D. P.; Dworkin, J. P.; Abe, C.; Nakamura, T. Extraterrestrial Ribose and Other Sugars in Primitive Meteorites.

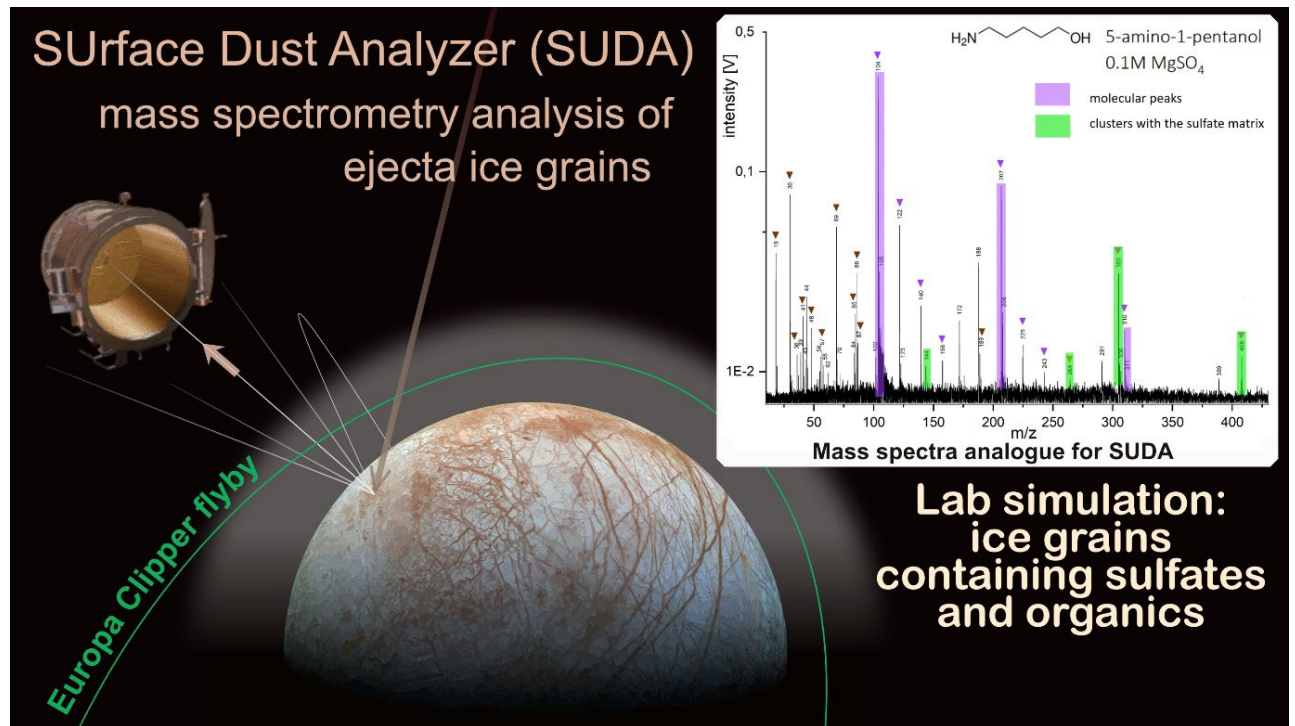
Proc. Natl. Acad. Sci. U.S.A. **2019**, *116* (49), 24440–24445.
<https://doi.org/10.1073/pnas.1907169116>.

(90) Rodriguez, L. E.; House, C. H.; Smith, K. E.; Roberts, M. R.; Callahan, M. P. Nitrogen Heterocycles Form Peptide Nucleic Acid Precursors in Complex Prebiotic Mixtures. *Sci Rep* **2019**, *9* (1), 9281. <https://doi.org/10.1038/s41598-019-45310-z>.

(91) Hand, K. P.; Carlson, R. W. Laboratory Spectroscopic Analyses of Electron Irradiated Alkanes and Alkenes in Solar System Ices: IRRADIATED HYDROCARBONS IN ICE. *J. Geophys. Res.* **2012**, *117* (E3), n/a-n/a. <https://doi.org/10.1029/2011JE003888>.

Table of Contents (TOC) Graphic

SURface Dust Analyzer (SUDA) mass spectrometry analysis of ejecta ice grains



Europa Clipper flyby

Intensity [V]

Mass spectra analogue for SUDA

m/z

0.5
0.1
1E-2

50 100 150 200 250 300 350 400

H2NCCCCCO 5-amino-1-pentanol
0.1M MgSO4

■ molecular peaks
■ clusters with the sulfate matrix

Lab simulation:
ice grains
containing sulfates
and organics